Atmospheric
Chemistry
and Physics
Discussions

Towards understanding the mechanisms of new particle formation in the Eastern Mediterranean

Rima Baalbaki[1], Michael Pikridas[2], Tuija Jokinen[1], Tiia Laurila[1], Lubna Dada[1], Spyros Bezantakos[2], Lauri Ahonen[1], Kimmo Neitola[1,2], Anne Maisser[2], Elie Bimenyimana[2], Aliki Christodoulou[2,3], Florin Unga[2], Chrysanthos Savvides[4], Katrianne Lehtipalo[1,5], Juha Kangasluoma[1], George Biskos[2], Tuukka Petäjä[1], Veli-Matti Kerminen[1], Jean Sciare[2], Markku Kulmala[1]

[1]Institute for Atmospheric and Earth System Research (INAR) / Physics, Faculty of Science, University of Helsinki, P.O. Box 64, Helsinki, 00014, Finland
[2]Climate & Atmosphere Research Centre (CARE-C), The Cyprus Institute, P.O. Box 27456, Nicosia, CY-1645, Cyprus
[3]IMT Lille Douai, Université de Lille, SAGE - Département Sciences de L'Atmosphère et Génie de L'Environnement, 59000, Lille, France
[4]Ministry of Labour, Welfare and Social Insurance, Department of Labour Inspection (DLI), Nicosia, Cyprus
[5]Finnish Meteorological Institute, Helsinki, Finland

Correspondence to: rima.baalbaki@helsinki.fi

Abstract

To quantify the contribution of new particle formation (NPF) to ultrafine particle number and CCN budgets, one has to understand the mechanisms that govern NPF in different environments and its temporal extent. Here, we study NPF in Cyprus, an Eastern Mediterranean country located at the crossroads of three continents. We performed one-year continuous measurements of aerosol particles down to ~ 1 nm in diameter, for the first time in the Eastern Mediterranean and Middle East (EMME) region. These measurements were complemented with trace gas data, meteorological variables and retroplume analysis. We show that NPF is a very frequent phenomenon at this site and has higher frequencies of occurrence during spring and autumn. NPF events were both of local and regional origin, and the local events occurred frequently during the month with the lowest NPF frequency. Some NPF events exhibited multiple onsets, while others exhibited particle apparent shrinkage in size. Additionally, NPF events were observed during the night-time and during episodes of high desert dust loadings. Particle formation rates and growth rates were comparable to those in urban environments, although our site is a rural one. Meteorological variables and trace gases played a role in explaining the intra-monthly variability of NPF events, but did not explain why summer month had the least NPF frequency. Similarly, pre-existing aerosol loading did not explain the observed seasonality. The month with the least NPF frequency were associated with higher H_2SO_4 concentrations but lower NO_x concentration, which is an indicator of anthropogenic influence. Air masses arriving from the Middle East were not observed during these month, which could suggest that precursor vapors important for nucleation and growth are transported to our site from the Middle East. Further comprehensive measurements of precursor vapors are required to prove this hypothesis.

1 Introduction

Atmospheric new particle formation (NPF) is the process by which oxidized precursor gases initially form molecular clusters that then further grow in size by multi-component condensation (Kulmala et al., 2014). A multitude of research studies have focused on this phenomenon over the past two decades because it is a large source of the global aerosol particle number and cloud condensation nuclei (CCN) load (Gordon et al.,

42 2017;Merikanto et al., 2009;Pierce and Adams, 2009;Wang and Penner, 2009;Yu and Luo, 2009;Kerminen et
43 al., 2012;Spracklen et al., 2006;Spracklen et al., 2008). Owing to the complex nature and non-linearity of
44 atmospheric processes, studies on NPF in the literature include atmospheric observations (e.g. Kulmala et al.,
45 2013;Ehn et al., 2014;Bianchi et al., 2016;Yao et al., 2018;Williamson et al., 2019;Baccarini et al.,
46 2020;Dall'Osto et al., 2018), chamber experiments (e.g. Sipilä et al., 2010;Tröstl et al., 2016;Wang et al.,
47 2020;Lehtipalo et al., 2016;Kirkby et al., 2011), and theoretical computational studies (e.g. Kurten et al.,
48 2008;Riipinen et al., 2011;Olenius and Riipinen, 2017). The collective scientific outcome from these studies
49 is essential to understand the mechanisms and characteristics of NPF (Kerminen et al., 2018;Lee et al.,
50 2019;Chu et al., 2019) and how it affects the global climate (e.g. Spracklen et al., 2006;Gordon et al., 2017).

51 The frequency, strength, and spatio-temporal extent of NPF are mainly governed by three factors: the
52 prevailing meteorological conditions, the availability of gaseous precursors and the pre-existing concentrations
53 of aerosol particles (Kerminen et al., 2018;Lee et al., 2019;Nieminen et al., 2018). These atmospheric
54 conditions differ in space and time. Atmospheric conditions are distinct over the Mediterranean basin,
55 especially over the Eastern Mediterranean and Middle East (EMME). This region has been identified as a
56 hotspot for atmospheric and climate change research (Lelieveld et al., 2016;Giorgi and Lionello, 2008). It is
57 surrounded by three continents and is affected by continental, maritime and desert-dust pollution sources
58 (Lelieveld et al., 2002). The surrounding complex orography of the Mediterranean affects atmospheric
59 dynamics and boundary layer processes on different scales (Kostopoulou and Jones, 2007b, a). Further, the
60 dry and hot weather throughout most of the year, with strongly increasing heat extremes, enables intense
61 photochemistry (Lelieveld et al., 2016).

62 NPF studies over the Mediterranean have focused on the north western basin (Petäjä et al., 2007;Cusack et al.,
63 2013;Berland et al., 2017;Carnerero et al., 2018;Rose et al., 2015;Brines et al., 2015;Hamed et al.,
64 2007;Laaksonen et al., 2005;Casquero-Vera et al., 2020), whereas NPF studies in the eastern basin have been
65 conducted mainly in Greece (Petäjä et al., 2007;Berland et al., 2017;Kalivitis et al., 2015;Kalivitis et al.,
66 2019;Pikridas et al., 2012;Kalkavouras et al., 2019;Kalkavouras et al., 2020;Kopanakis et al., 2013;Siakavaras
67 et al., 2016;Kalkavouras et al., 2017) and very recently in Cyprus (Brilke et al., 2020;Debevec et al., 2018)
68 and Jordan (Hussein et al., 2020). These studies include both short-term campaigns and long-term observation.

69 Based on long-term measurements, the annual frequency of NPF over the Mediterranean varies between 10
70 and 36% (Hussein et al., 2020;Kalivitis et al., 2019;Kalkavouras et al., 2020;Kopanakis et al., 2013). The
71 seasonal cycle has a typical maximum during spring (Kalkavouras et al., 2020;Kopanakis et al., 2013;Kalivitis
72 et al., 2019;Pikridas et al., 2012), even though in some urban background sites the highest frequency was
73 observed during summer (Hussein et al., 2020;Hamed et al., 2007). NPF was associated with a high increase
74 in nucleation mode particles in most of the studies. For instance, Carnerero et al. (2018) showed that the impact
75 of NPF on ultrafine particles is much higher than that of traffic near the highly polluted city center of Madrid.
76 The condensation sink, which is a measure of the pre-existing aerosol surface area, was reported to be lower
77 during NPF events in Po valley, Corsica and Crete (Hamed et al., 2007;Berland et al., 2017;Pikridas et al.,
78 2012), while NPF proceeded under both clean and polluted conditions in Barcelona (Cusack et al., 2013),
79 Marseille and Athens (Petäjä et al., 2007). The effect of meteorological conditions on NPF occurrence varied
80 among studies. Simultaneous NPF events were observed in several stations, illustrating that the spatial extent
81 of NPF events can vary from tens of kilometers (Carnerero et al., 2018) to several hundred kilometers
82 (Kalkavouras et al., 2017;Kalkavouras et al., 2020;Berland et al., 2017;Rose et al., 2015;Casquero-Vera et al.,
83 2020). In the Po valley, the production of CCN from NPF was estimated to be comparable to that originating
84 from primary sources (Laaksonen et al., 2005). Similarly, NPF was associated with a strong increase in CCN
85 concentrations in Finokalia and Santorini (Kalkavouras et al., 2019;Kalkavouras et al., 2017;Kalivitis et al.,
86 2015). However, the impact of the increased CCN concentrations on cloud droplet number was shown to be

Atmospheric
Chemistry
and Physics
Discussions

Open Access

EGU

87   limited by water availability (Kalkavouras et al., 2017). In Cyprus, mainly in Paphos, Gong et al. (2019)
88   observed several NPF events where newly-formed particles grew into the CCN size range, with NPF events
89   being observed on 9 out of 27 measurement days during April 2017 (Brilke et al., 2020). At a more inland
90   site, NPF was observed on 14 out of 20 days of measurements on March 2015 (Debevec et al., 2018). Since
91   these studies were less than a month long, further comprehensive measurements are required to unveil the role
92   of NPF in the atmospheric processes taking place in the EMME region.

93   The aim of this study is to characterize the seasonal cycle of new particle formation events in the less
94   represented area of the EMME region. Our measurements were conducted at a rural background site on the
95   island of Cyprus which lies at the crossroads of three continents in the Eastern Mediterranean. We report the
96   first long-term analysis of particle number size distribution in the area, down to sizes where the initial
97   formation occurs. We further explore the role of sulfuric acid, which is the key gas phase precursor for cluster
98   formation, and other atmospheric variables in initiating NPF at this site.

2   Materials and Methods

2.1 Measurement site

Cyprus is an island country in the Eastern Mediterranean. It is the most populated island in the Mediterranean Sea, and the third largest in size with an area of 9251 km^2. Cyprus is surrounded by Turkey from the north, Syria and Lebanon from the east, Egypt from the south, and Greece from the west/northwest (Figure 1). The measurements reported in this work were carried out at the Cyprus Atmospheric Observatory (CAO; Sciare, 2016), which is a rural background station that operates under the co-operative programme for monitoring and evaluation of the long-range transmission of air pollutants in Europe (EMEP) and the European Research Infrastructure for the observation of Aerosol, Clouds and Trace Gases (ACTRIS) networks, while at the same time it is a designated regional Global Atmospheric Watch (GAW) station. The CAO site (35.038692° N, 33.057850 ° E) is located close to the villages of Agia Marina (≈630 inhabitants) and Xyliatos (≈150 inhabitants) and has an elevation of 532 m above sea level. The proximity of the site is surrounded by vegetation mainly oak and pine trees and Maquis shrubland as it lies at the northern-eastern foothills of the Troodos Mountains. Agriculture areas surround the site from the north direction and are approximately 4 km away. The nearest main urban agglomeration is at least 35 km away. Therefore, it is distant from any major pollution sources, excluding some limited traffic to reach the nearby Forestry Department premises.

The weather at CAO is characterized by hot dry summers and mild, rainy winters. The daily mean temperature is ~19°C and ranges between 1 and 36°C, the daily mean relative humidity is ~55% and ranges between 13 and 82%, and the daily mean ozone level is ~48 ppb, ranging between 26 and 77 ppb (Kleanthous et al., 2014). The most common (> 65% occurrence) wind pattern reaching the site is the northerly "Etesian" winds transporting pollutants from both Europe and Turkey, but more frequently from mainland of Turkey (Pikridas et al., 2018).The remaining air masses originate from North Africa, the Middle East and westerlies air masses that spend several days above the sea before reaching Cyprus. The variable air mass origins at CAO from three different continents allow a representative description of NPF processes for the EMME region as a whole.

[Figure 1 goes here]

2.2 Instrumentation

2.2.1   Aerosol particle number size distribution

The particle number size distribution between 1 and 700 nm was determined by combining data from three instruments: an Airmodus A11 Nano Condensation Nucleus Counter (nCNC) system (Vanhanen et al., 2011), a Neutral cluster and Air Ion Spectrometer (NAIS Model 1; Manninen et al., 2016;Mirme and Mirme, 2013), and a Scanning Mobility Particle Sizer (SMPS Model TSI 3080; Wang and Flagan, 1990). The first two instruments were operated at the site for a period of one year from January 27, 2018 to January 26, 2019 while the SMPS measurement period was from January 27, 2018 to November 1, 2018. The monthly availability of data from each instrument is shown in Table S1.

The A11 nCNC is composed of a Particle Size Magnifier (PSM; Airmodus A10) and a Condensation Particle Counter (CPC; Airmodus A20). The overall length of the inlet sampling tube was 60 cm. The PSM was operated in a scanning saturator flow mode between 0.1 and 1.3 liter per minute (lpm), corresponding to a cut-off diameter range of approximately 1.1 to 2.5 nm. It was equipped with an inlet system that performs background (zero) measurements three times a day at random time intervals, and a core sampling piece for minimizing line losses of sub-3 nm particles (Figure S1). The duration of the background measurements was set to 12 minutes, which is equivalent to 3 full size scans. From June 2018 onwards, the PSM was additionally equipped with a diluter to reduce the humidity of the sampled air. This procedure was necessary because the water content of the air at the measurement site was too high, and it affected the activation efficiency inside

142 the CPC and therefore distorted the size distribution measurements for the smallest sizes. Further information
143 about the diluter design and operation can be found in the supplementary information (SI) Sect. 2.2.

144 The NAIS is a mobility spectrometer designed to determine the number size distribution of ions in the mobility
145 diameter range of 0.8 – 42 nm, as well as total (naturally charged and neutral) aerosol particles in the mobility
146 diameter range of ~2 – 42 nm. The instrument operates at the flow rate of ~54 lpm. The length of the NAIS
147 sampling tube was 65 cm, with an inner diameter of 30 mm.

148 The SMPS used in this study was composed of a TSI 3081 long Differential Mobility Analyzer (DMA) and a
149 TSI 3025a CPC. It was operated to measure the aerosol particle size distribution between 15 and 740 nm. The
150 aerosol and sheath flow were checked weekly and were set to 0.3 and 3 lpm, respectively. The SMPS was
151 sampling using an 80-cm long vertical inlet. Drying was achieved using a short nafion dryer, and charge
152 neutralization was achieved by a GRIMM 5522-A, Americium-241, bipolar neutralizer.

2.2.2   Ancillary measurements
154 Complementary meteorological data (temperature, relative humidity, solar radiation, rainfall, pressure, wind
155 speed and wind direction) were measured at an elevation of 10 m from the ground at the nearby village of
156 Xyliatos (35.0140917 N, 33.0492028 E), 2.85 km from the measurement site. Air pollutants (ozone, carbon
157 monoxide, nitrogen oxides, sulfur oxide, PM_{10} and $PM_{2.5}$) were measured at the collocated EMEP station ~20
158 m from the main measurement container. Additional details about the set-ups and the instrument used can be
159 found in Kleanthous et al. (2014) and Pikridas et al. (2018).

2.3 Data handling
161 *nCNC:* The scanning nCNC data was inverted into a size distribution with the Kernel inversion method
162 presented by Lehtipalo et al. (2014), but using customized kernels which follow the instrument specific
163 detection efficiency calibration curves. The choice of the inversion method was made after a comprehensive
164 comparison between the Kernel method and the Expectation and Minimization (EM) method (Cai et al.,
165 2018;Chan et al., 2020). Additional details about the comparability of the two methods and the utilized
166 inversion parameters are presented in Sect. 2.3 of the SI. After inversion, the data were further corrected for
167 line losses using the method suggested by Fu et al. (2019) for the sampling line downstream of the core
168 sampling inlet, and using the Gormley and Kennedy equation for the line losses inside the 6-cm-long core
169 sampling piece (Gormley and Kennedy, 1948).

170 *NAIS:* The NAIS data were inverted with the instrument specific algorithm (done by the NAIS SPECTOPS
171 software). The data were later corrected for line losses using the Gormley and Kennedy equation for laminar
172 flow (Gormley and Kennedy, 1948). It is essential to note that the flow through the sampling inlet of the NAIS
173 actually lies in the transient regime (Re = 2376), however the penetration efficiency using this inlet was
174 comparable for laminar flow and turbulent flow (calculated using the equation of turbulent inertial deposition
175 from Brockmann (2011)), thus we used the correction based on laminar flow (Figure S3).

176 *SMPS:* The data from the SMPS were inverted using the TSI's Aerosol Instrument Manager (AIM, version
177 9.0) software. Afterwards, line loss correction was applied using Gormley and Kennedy equation. Additional
178 corrections based on lab calibrations were also applied to account for the low CPC detection efficiency below
179 15 nm.

180 *Full Particle Size Distribution (PSD):* The data from the three particle sizing instruments were used to
181 reconstruct the full particle size distribution between 1.1 and 736 nm (nCNC: 1.1 to 2.4 nm; NAIS particle
182 mode: 2.4 to 30 nm; SMPS: 30 to 736 nm). However, since the NAIS is known to overestimate concentrations
183 in particle mode, the overlapping measurement range with the SMPS was used to further correct the NAIS

184   data assuming that the NAIS overestimate concentrations uniformly over the whole measurement range, which
185   is a reasonable assumption for old NAIS models based on calibration results (Gagné et al., 2011;Kangasluoma
186   et al., 2020). Additionally, the SMPS measured dry aerosol particle number distributions, which can differ
187   considerably from the ambient aerosol particle number size distribution. Thus, we back-calculated the
188   distribution at ambient conditions from the dry distribution using the hygroscopicity model of Petters and
189   Kreidenweis (2007) and mean kappa values. Additional information about these calculations and its effect on
190   sink calculations are presented in Sect. 4 of the SI material. The full PSD using the distribution at ambient
191   conditions was reconstructed up to 1500 nm. This does not imply that the measurement range was extended to
192   1500 nm, but rather that now we account for particles that were originally of sizes up to 1500 nm but were
193   dried to sizes below 740 nm in the SMPS sampling line. Finally, the PSD data was run through a 2D median
194   filtering algorithm with a 3-by-3 neighborhood window. Moreover, the data was manually checked for the
195   success of the outlier and noise removal techniques.

196   *Complementary data:* Gas and meteorology data sets were run through an outlier removal algorithm and
197   filtered for erroneous samples. The outlier detection method was based on removing data points that are more
198   than three standard deviations from a moving median (Davies and Gather, 1993;Pearson et al., 2016).

199   **2.4 Event classification**
200   The reconstructed full particle size distribution daily plots were used to categorize measurement days into NPF
201   event days, non-event days and undefined days based on a classification that combines the schemes reported
202   in literature (Dal Maso et al., 2005;Hirsikko et al., 2007;Manninen et al., 2010;Kulmala et al., 2012). The
203   classification of events utilizing PSD data that extends below 10 nm, which is a typical measurement limit for
204   most SMPS systems, improves the event classification and allows better identification of event days that would
205   otherwise be classified as undefined or non-events if only PSDs above 10 nm were used (Leino et al.,
206   2016;Dada et al., 2018;Brilke et al., 2020). In addition, spectrums of total particles (both neutral and charged)
207   are usually less ambiguous to classify than charged particle spectra (ion mode of NAIS), and the classification
208   of event days may be different if one only looks at these charged spectrums.

209   **2.5 NPF specific parameters**
210   *Condensation sink (CS)* is a loss term for condensable vapors used to describe their loss rate by condensation
211   to pre-existing aerosol surface. This term was first introduced by Kulmala et al. (2001) and it is derived based
212   on condensing vapor mass flux to the particles in the continuum regime and applying the transitional correction
213   factor (β_m) proposed by Fuchs and Sutugin (1971):

$$\text{CS} = 4\pi D \sum_i \beta_{m_i} r_i N_i = 2\pi D \sum_i \beta_{m_i} d_{p_i} N_i , \qquad (1)$$

215   where r, d_p and N are the particle radius, diameter and number concentration, respectively, in the size class i,
216   and D is the diffusion coefficient of the condensing vapor calculated as recommended by Fuller et al. (1966):

$$D(H_2SO_4, air) = \frac{0.001 T^{1.75} \sqrt{\dfrac{1}{M_{H_2SO_4}} + \dfrac{1}{M_{air}}}}{P \left(\sqrt[3]{V_{H_2SO_4}} + \sqrt[3]{V_{air}} \right)^2} , \qquad (2)$$

218   where T is the temperature, M is the molar mass, P is the atmospheric pressure, and V is the diffusion volume.
219   Here, CS was calculated assuming that sulfuric acid is the main condensing vapor.

220 *Coagulation sink (CoagS)* is a loss term for freshly formed particles used to describe their loss rate by
221 Brownian coagulation to pre-existing aerosol surface (Kulmala et al., 2001). It is calculated as:

$$CoagS(d_p) = \sum_j K_{ij} N_j \ ,$$ (3)

223 where K_{ij} is the Fuchs form of the Brownian coagulation coefficient (Fuchs, 1964;Seinfeld and Pandis, 2012).

224 *Growth rate (GR)* is the rate of change in the diameter, d_p, that represents the growing particle population. It
225 was calculated here using the NAIS negative ion mode data by first finding the time of the maximum
226 concentration at each diameter measured by the NAIS (maximum concentration method) (Kulmala et al., 2012)
227 and then deriving the growth rate as the slope of the linear fit between the diameters and time:

$$GR = \frac{dd_p}{dt} = \frac{\Delta d_p}{dt}.$$ (4)

229 We calculated GR at three different size ranges: between 1.5 and 3 nm ($GR_{1.5-3}$), between 3 and 7 nm (GR_{3-7})
230 and between 7 and 20 nm (GR_{7-20}).

231 *Event start and end times* were determined based on the time evolution of the 2-4 nm particles which is the
232 size range suggested by Dada et al. (2018). Using this size range, we are able to capture the early stages of the
233 event which is unachievable if the measured PSD starts from bigger sizes. Thus, computed event start and end
234 times might differ across studies depending on the instrument used.

235 *Particle formation rate (J)* is the rate at which aerosol particles of certain size are formed in the atmosphere.
236 It quantifies the intensity of the NPF events, and it is calculated by rearranging the equation describing the
237 time evolution of the particle number concentration (Kulmala et al., 2012). Dp in this equation refers to the
238 smaller limit of the size bin used in the calculation of the formation rate. We calculated J at three sizes: 1.5 nm
239 ($J_{1.5}$), 3nm (J_3) and 7nm (J_7); the upper size limits used were 3, 7 and 20 nm, respectively. GR was considered
240 constant within the event start and end times. Outside the event times and during non-events the GR term was
241 considered equal to zero.

$$J_{dp} = \frac{dN_{d_p}}{dt} + CoagS\ N_{d_p} + \frac{GR}{\Delta D_p} N_{d_p},$$ (5)

243 where the first term in represents the time evolution of particle number concentration N_{d_p}, the second term
244 represents the coagulation losses due to larger aerosol particles, and the third term represents the
245 condensational growth to sizes bigger than the considered size range.

246 **2.6 Sulfuric acid proxy**
247 Sulfuric acid is one of the key gas-phase compounds identified to contribute to new particle formation (e.g.
248 Weber et al., 1996;Sipilä et al., 2010). As direct measurements of sulfuric acid is challenging, a suite of proxies
249 for the sulfuric acid concentrations are derived that facilitate calculation of gas phase sulfuric acid from
250 ancillary observations (Dada et al., 2020;Mikkonen et al., 2011;Petäjä et al., 2009;Lu et al., 2019;Weber et al.,
251 1997). In this study, the sulfuric acid proxy was calculated using the new method by Dada et al. (2020) for a
252 rural site, which was developed based on observations from the same site of this study :

$$[H_2SO_4]_{rural} = -\frac{CS}{2\ x\ (2\ x\ 10^{-9})} + \left[\left(\frac{CS}{2\ x\ (2\ x\ 10^{-9})} \right)^2 + \frac{[SO_2]}{(2\ x\ 10^{-9})} (9\ x\ 10^{-9}\ x\ GlobRad) \right]^{\frac{1}{2}}$$ (6)

254   This proxy does not only consider the formation of H_2SO_4 from SO_2 via OH oxidation and the loss towards
255   pre-existing particles (condensation sink), but also includes the formation pathway via stabilized Criegee
256   Intermediates and loss towards atmospheric clustering starting from H_2SO_4 dimer formation.

257   **2.7 Air mass origin analysis**
258   Air mass origins for the entire measurement period were modeled using the Lagrangian particle dispersion
259   model FLEXPART (FLEXible PARTicle dispersion model), version 8.23, in a backward mode (Stohl et al.,
260   2005), with meteorological (0.5x0.5°, 6 h starting from midnight UTC) NCAR (ds 0.94) data as input. We
261   used "species" 1 (tracer), which do not include wet or dry deposition and assumes an infinite lifetime for the
262   particles, as the tracer released to model the retroplumes. Retroplumes replaces simple back trajectory
263   calculations in the interpretation of atmospheric trace substance measurements, and were traced back in time
264   for 5 days using CAO as the receptor site. Air masses were categorized to source regions based on the potential
265   emission sensitivity (PES) for the lowest 1 km above ground level (agl), following the classification method
266   of Pikridas et al. (2010). Seven source regions were identified similar to the ones presented by Pikridas et al.
267   (2018) except that in our analysis, the West Turkey sector was merged to the NW Asia sector.

268   **2.8 Identification of days with high dust loading**
269   Measurement dates with high dust loading were identified using the VI-PM1 online method proposed by
270   Drinovec et al. (2020). This method couples a high-flow virtual impactor (VI) sampler, which concentrates
271   coarse particles, with an aerosol absorption photometer. More details about the calculations and a list of the
272   identified dust days can be found in Sect. 5 of SI.

3   Results and Discussion

In the course of identifying NPF events, the PSD spectrum is usually analyzed, mainly at sizes below 25 nm where one can detect the emergence of new aerosol particles, and then the particle growth to larger sizes is followed. Since little is known about particle number size distributions from the EMME region, we will first present the seasonal and diurnal variability of particle number concentration in different PSD modes (Sect. 3.1). Then, we will identify and characterize NPF events (Sect. 3.2). Following, we will quantify and analyze relevant parameters that describe NPF events (Sect. 3.3) and use those parameters, together with meteorological variables, to understand why and when NPF occurs at our site (Sect. 3.4). All the data in this manuscript are presented in local time (UTC+3 from 25 March 2018 to 28 October 2018, and UTC+2 during the rest of the campaign). Unless otherwise indicated, we mainly focus on daytime data having global radiation > 50 W m^{-2} because it is the time period relevant for most NPF events, but we also briefly mention some night-time events. For reference, the monthly range of day hours having global radiation > 50 W m^{-2} is presented in Figure S5.

3.1 Seasonal and diurnal variability of number concentration in different modes

Figure 2 presents the monthly percentiles boxplots (25th, 50th and 75th) and the mean averages of the cluster mode [~1–3 nm], nucleation mode [3–25 nm], Aitken mode [25–100 nm] and accumulation mode [100-1000 nm] particle number concentrations computed from daily data with global radiation > 50 W m^{-2} (daytime conditions). A clear seasonal pattern is depicted which is distinct across the different particle modes. The cluster mode and nucleation mode particles had roughly a similar pattern, with the highest concentrations during the spring followed by the autumn and a clear drop during the summer. The cluster and nucleation mode concentrations can be directly linked to the NPF activity, especially in sites where direct emissions of particles having these size ranges are minimal, which is the case for our site. The Aitken mode exhibited higher concentrations during the spring months followed by a decreasing pattern, which could either suggest more growth from NPF to Aitken sizes or higher emission during spring. The accumulation mode had its maximum during the summer, except during July which did not follow the pattern of other months. Previous long-term measurements of PM$_{2.5}$ at this site have a similar pattern with higher concentrations during the warm period of the year and minimum during winter (Pikridas et al., 2018). This maximum during the summer is mainly explained by the enhanced transport of polluted air masses from the north sector, combined with the lack of precipitation and overall dry conditions during Eastern Mediterranean summer (Pikridas et al., 2018).

[Figure 2 goes here]

The diurnal variation (at radiation > 50 W m^{-2}) of the cluster and nucleation mode particles exhibited a clear cycle, with the highest values recorded between 9:00 and 15:00 am and the maximum at 11:00 (Figure S6 a & b). The Aitken mode had a less distinct diurnal cycle having the peak at later hours of the day, which might indicate that these particles have possibly grown from the cluster and nucleation modes (Figure S6.c). The accumulation mode, on the other hand, did not exhibit any clear diurnal cycle, which might suggest that these particles are not emitted or produced from any local source but are rather long-range transported. They can be aged primary particles, or particles originating from NPF taken place 1-3 days earlier in arriving air masses (Figure S6.d).

3.2 General character of the NPF events

New particle formation has been detected to occur in a variety of environments within the troposphere (Kerminen et al., 2018;Lee et al., 2019;Nieminen et al., 2018). Typically, the appearance of clusters is detected in the morning hours followed by subsequent growth. The occurrence of new particle formation events is determined by examining the time evolution of the aerosol number size distributions (e.g. Kulmala et al., 2012). An example of such events is presented in Figure S7. Throughout the one-year measurement campaign (365 days), 207 (56.7 %) days were identified as event days, 119 (32.6 %) days were identified as non-event days,

318   31 (8.5 %) days were undefined days and 8 (2.2 %) days did not have data mainly due to power cuts at the

319   station (Figure 3). The annual-median NPF frequency at CAO calculated without accounting for days with no

320   data amounts to 58% which belongs to the high end of the global NPF frequency distribution (Nieminen et al.,

321   2018) with the highest frequency being measured in South Africa (86%; Hirsikko et al., 2012). High frequency

322   of NPF occurrence is also observed at Saudi Arabia (73%; Hakala et al., 2019)

323   NPF took place throughout the year at CAO, but it had a clear seasonal pattern with a broad spring maximum,

324   less pronounced autumn maximum, and slightly lower frequencies during other times of the year. The months

325   with the highest NPF frequencies were March and April, while June and August had the lowest frequencies.

326   This seasonal pattern of NPF frequency is very similar to that recorded at the Finokalia atmospheric

327   observation station in Crete, Greece (Kalivitis et al., 2019) which is a nearby Eastern Mediterranean site having

328   similar synoptic conditions. Nonetheless, monthly NPF frequency at Finokalia ranged between ~17 and 42%

329   which is substantially lower than the range reported here for CAO (33 - 86%). The higher NPF frequency at

330   CAO could partially be due to the use of PSD data that starts from the ~1-nm size range, which facilitates NPF

331   classification especially during days when the particle growth does not pass the 10-nm size or does not continue

332   for several hours. We compared the NPF classification using SMPS data only and that using full PSD for time

333   periods when SMPS data were available, and attained 30 % less event days classified. Another factor that

334   could contribute to the higher NPF frequency at CAO is the surrounding forest nature which emits VOCs that

335   oxidize in the atmosphere and contribute to particle growth (Riipinen et al., 2011).

336   [Figure 3 goes here]

337   We further separated the NPF event days into class I or class II events, or into the so-called "bump" events

338   (Manninen et al., 2010). Examples of these event types are given in Figure S7. Class I events differ from class

339   II events not by the strength of the event but rather by the ability to calculate the particle growth rate for such

340   event, meaning that the growing mode diameter or concentration does not fluctuate strongly. Bump events are

341   NPF events where a burst of nucleation mode particles is seen but the particles do not usually grow past the

342   ~10-nm size, and the duration of these events is typically short. The calculation of growth rates for these events

343   is sometimes problematic because the growth happens very fast (in less than 15 minutes) and it cannot be

344   captured by the time resolution of the measuring instrument. In the literature, these events have been called

345   "bursting events" (Dall´Osto et al., 2017), "hump events" (Vakkari et al., 2011;Yli-Juuti et al., 2009),

346   "suppressed events" (Chen et al., 2017), "stationary NPF events" (Größ et al., 2018) or "weak NPF events"

347   (Lee et al., 2020). The fraction of these events were highest during the month with the lowest NPF frequency

348   (mainly during summer), which could imply that during these months less amount of condensing vapors was

349   present to grow the particles to bigger sizes or extend the event duration (Figure 4).

350   [Figure 4 goes here]

351   The NPF events started almost always from the sub-3-nm range at CAO. The apparent growth reached a

352   diameter of 20 nm on 25% of event days (Figure 5a), thus it could have been difficult to identify those days if

353   we have relied solely on SMPS measurements which suffer from high losses and low counting statistics in the

354   sub-10-nm size range (Brilke et al., 2020;Kangasluoma et al., 2020;Wiedensohler et al., 2012). Additionally,

355   it was difficult to distinguish the growing mode at sizes above 50 nm mainly because of background aerosols

356   and fluctuating air masses. This implies that particles growing from NPF might have been able to grow to

357   bigger sizes, but their identification from the PSD spectrum was not possible. The median event duration was

358   ~ 5.4 hours (Figure 5b). The events typically started two to four hours after sunrise and ended seven to eleven

359   hours after sunrise (Figure 5c), similar to what was observed by Dada et al. (2018).

360   [Figure 5 goes here]

361   Another feature of NPF events observed at CAO was the occurrence of two or three consecutive daytime
362   nucleation events (Figure 6). These multiple events occurred on ~20% of the recorded event days. Similar
363   observations were reported in South Africa, and they were mainly attributed to changes in air masses,
364   interruptions by clouds and boundary layer dynamics and its relation to the amount of vapors present (Hirsikko
365   et al., 2013). Salma and Németh (2019) have also showed that NPF events with broad or multiple onsets are
366   abundant in the urban environment of Budapest, Hungary.

367   We also observed events with a decreasing mode diameter, sometimes referred to as shrinkage events. These
368   events were mainly observed in the NAIS ion mode, while some of them were also observed in both ion and
369   total particle spectrum (Figure 7). These types of events have been observed in multiple environments and are
370   usually attributed to particle evaporation triggered by elevated temperatures, size-dependent dilution by wind-
371   or boundary layer development-mixing, or changes in air masses bringing small particles to the measurement
372   site (Alonso-Blanco et al., 2017;Backman et al., 2012;Cusack et al., 2013;Hakala et al., 2019;Kivekäs et al.,
373   2016;Salma et al., 2016b;Skrabalova et al., 2015;Tsagkogeorgas et al., 2017;Yao et al., 2010;Young et al.,
374   2013;Zhang et al., 2016;Carnerero et al., 2018).

375   We spotted a few events with nighttime clustering, which could reflect a chemistry that does not depend on
376   photo-oxidation (Figure 8). These events occurred mainly during the cold months associated with high cluster
377   mode concentration. Nighttime events have been observed in other Mediterranean studies as well (Carnerero
378   et al., 2018;Kopanakis et al., 2013;Kalivitis et al., 2012). In a boreal forest, nighttime clustering events that do
379   not usually grow past 5 nm have been attributed to the formation of large highly-oxygenated organic molecules
380   (HOM) mainly from monoterpene oxidation (Lehtipalo et al., 2011;Rose et al., 2018;Bianchi et al., 2019). In
381   the French Landes forest, nocturnal NPF events with clear growth up to 100 nm were attributed to monoterpene
382   oxidation under stratified atmospheric conditions (Kammer et al., 2018). Monoterpenes concentrations
383   reported at the Landes forest reached up to 25 ppb, whereas those reported in the boreal forest were below 2
384   ppb. Concurrent measurements of biogenic volatile organic compounds (BVOCs) were not available in this
385   study but the average concentration of monoterpenes during March 2015, which is a month with high biogenic
386   activity, was reported to be 0.236 ± 0.294 ppb with a maximum up to 4.5 ppb (Debevec et al., 2018).

387   Lastly, the EMME region is characterized by a high loading of dust which contributes to around 34% (~10
388   μgm^{-3}) of the annual PM_{10} levels (Pikridas et al., 2018). Desert dust storms occur more frequently during late
389   winter and spring (Achilleos et al., 2014;Pikridas et al., 2018). In this study, fifty days with high dust loading
390   (Table S3) were identified based on ground measurements of mineral dust concentrations (Sect. 5 of SI).
391   Among these dates, 37 were NPF event days, 9 were non-events, 2 were undefined and 2 had no data. Thus,
392   high dust loading (translated to a high condensation sink) does not seem to suppress NPF. On the contrary, Nie
393   et al. (2014) have suggested earlier that heavy dust plumes could be an unexpected source of nucleating and
394   condensable vapors via dust-induced heterogeneous photochemical processes. Further investigation is required
395   to prove this suggestion for our site.

3.3 NPF specific parameters
397   In this section we analyze three parameters related to NPF: particle formation rates (J), particle growth rates
398   (GR) and condensation sink (CS). J and GR describe the strength of NPF, while CS is a measure of the sink
399   for both vapors contributing to NPF and small growing clusters. Taken together, these three quantities
400   eventually determine how efficiently NPF contributes e.g. to atmospheric CCN production.

401   *Particle formation rates:* The particle formation rates for 1.5, 3 and 7 nm particles ($J_{1.5}$, J_3 and J_7, respectively)
402   were calculated and they are presented in Table 1(daily data) and Table S4 (hourly data). $J_{1.5}$ was the highest
403   during the spring: March had the highest median $J_{1.5}$ while April had more events with extreme $J_{1.5}$ values as
404   expressed by the higher mean. We were not able to calculate formation rates later than the 2nd of November

405 because SMPS measurements were not available, but the pattern of $J_{1.5}$ seems to exhibit another peak during
406 the autumn, which is similar to the seasonal pattern of the NPF frequency and cluster mode concentration. In
407 contrast, J_3 and J_7 did not exhibit a clear seasonality, but their values were in general higher during the spring.
408 The diurnal cycle for the formation rates was more pronounced during the Class I events than during the Class
409 II or bump events, and the peak median hourly value was highest during Class I events (Figure 9). The median
410 peak of $J_{1.5}$ and J_3 during the class I events and bump events occurred between 11:00 and 12:00, whereas for
411 J_7 the peak occurred between 12:00 and 14:00. For the Class II events the corresponding peaks occurred about
412 1 hour later. To place the formation rates in global perspective, we compare J_3 from this study to other studies
413 (Table 2), because it is the most commonly reported value in literature. The studies in Table 2 were selected
414 on the basis of having one year or more of measurement data. J_3 determined in this study was up to a one order
415 of magnitude higher than that measured at semi-pristine rural areas (Värrio, Hyytiälä, and Tomsk), lower than
416 that measured in a megacity (Beijing) and comparable to values reported at urban and rural sites affected by
417 urban pollution (Budapest, Vavihill, and Po Valley).

418 *Growth rates:* We report size-segregated growth rates between 1.5 and 3 nm ($GR_{1.5-3}$), between 3 and 7 nm
419 (GR_{3-7}), and between 7 and 20 nm (GR_{7-20}) as recommended by Kulmala et al. (2012) (Table 3). The median
420 growth rates in these size ranges were 2.0, 4.8, and 7.4 nm hr^{-1}, respectively. These GRs are higher than those
421 reported for a rural boreal environment (1.9, 3.8 and 4.3 nm hr^{-1}, respectively) (Yli-Juuti et al., 2011), but
422 within the range of GRs reported for 12 European sites (Manninen et al., 2010 cf. Figure S8). The increase in
423 the growth rate with an increasing particle size is a typical feature in the sub-20 nm size range because
424 condensational growth is more favorable as the particle size increases and the Kelvin effect decreases
425 (Manninen et al., 2010). Additionally, we calculated the growth rates between 3 and 25 nm (GR_{3-25}) for the
426 purpose of making comparison with additional studies. Similar to J_3, the median GR_{3-25} calculated here (6.3
427 nm hr^{-1}) was comparable to the range reported for urban or rural sites with urban influence ($4.7 - 7.7$ nm hr^{-1}),
428 whereas rural sites usually have a GR_{3-25} below 4 nm hr^{-1}. In regard to the seasonal variability, we did not find
429 a clear pattern in GR_{7-20} or GR_{3-25}. In contrast, $GR_{1.5-3}$ and GR_{3-7} were generally higher during the summer
430 months, which could be associated to the higher fraction of bump events with respect to other event types. As
431 discussed in Sect. 3.3, these bump events are characterized by a burst of particles within a short period of time,
432 which would translate to higher growth rates.

433 *Condensation sink:* The median of CS at CAO, for the periods that SMPS measurements were available, was
434 7.9×10^{-3} s^{-1} (25th - 75th percentiles = $5.2 \times 10^{-3} - 13.9 \times 10^{-3}$) while the mean was 10.7×10^{-3} s^{-1} $\pm 8.2 \times 10^{-3}$ s^{-1}
435 (computed from daily median values). These values lie within the range of coastal (Kalivitis et al., 2019) and
436 urban environments (Salma et al., 2016a;Jun et al., 2014). They are higher than the values reported for forests
437 and semi-pristine environments (Dal Maso et al., 2002;Dada et al., 2017), and lower than the values reported
438 for highly polluted cities (Wu et al., 2007). The average diurnal cycle of the size segregated CS for the whole
439 measurement period shows that particles above 50 nm were the main contributors to the CS, even though
440 particles down ~3 nm could also exhibit a high CS (Figure S9). Thus, nucleating aerosols can largely contribute
441 to the available aerosol surface area. The seasonal variation of the CS followed the seasonal pattern of the
442 accumulation mode particles with highest values calculated for winter and spring, and lowest for summer and
443 autumn. This pattern does not follow the pattern reported from measurements carried out at Finokalia (Kalivitis
444 et al., 2019), where the highest values were calculated during the summer and autumn (Table S5). More
445 analysis about the seasonal variation of CS, especially with respect to NPF events, will be presented in the
446 Sect. 3.4.

3.4 The driving atmospheric parameters of the NPF events
448 To explain the occurrence of NPF at CAO, we investigated the effect of the following variables: CS,
449 meteorological conditions (temperature, solar radiation, pressure, relative humidity, wind speed and wind

450   direction), trace gas concentrations (NO_x, SO_2, CO and O_3), air mass origin and sulfuric acid – formation rate
451   relationship.

452   The NPF frequency typically decreases with an increasing CS (Pikridas et al., 2012;Salma et al., 2016a;Dada
453   et al., 2017;Dai et al., 2017;Hakala et al., 2019;Hussein et al., 2020). However, NPF has been observed in
454   polluted environments at exceptionally high values of CS, indicating that inefficient cluster scavenging or
455   enhanced cluster growth or a combination of both drives NPF regardless of the high load of pre-existing
456   particles (Yao et al., 2018;Kulmala et al., 2017). In our study, we did not find a clear relation between CS and
457   the monthly NPF occurrence, and NPF did not necessarily occur at low values of CS (Figure 10). To further
458   explore the effect of CS on NPF, we checked out whether the NPF event days had lower CS before the onset
459   of nucleation (period from midnight to morning) in comparison to non-event days, but we did not find any
460   apparent association (Figure S10).

461   Next, we inspected the effect of meteorological variables (Figure 11) on the occurrence of NPF. By considering
462   the data from all the months together, NPF events took place over a wide range of meteorological conditions.
463   Higher temperatures seemed to be favorable for intra-monthly NPF occurrence, however the higher
464   temperatures from June to September did not coincide with higher NPF frequencies (Figure 11a). The effect
465   of temperature on NPF has been studied extensively in chamber experiments, with a general consensus that
466   lower temperatures favor nucleation at the kinetic regime and thus enhance NPF in inorganic systems like the
467   sulfuric acid-ammonia system (Lee et al., 2019). However, in organic systems where highly oxygenated
468   organic compounds (HOM) are the main NPF species, temperature plays a double role. On the one hand, the
469   Gibbs free-energy barrier is reduced at lower temperatures, favoring the condensation of less oxidized vapors
470   that would not condense at higher temperatures. On the other hand, lower temperatures lead to decreased auto-
471   oxidation reaction rates and reduced yields of HOM. Recent studies have shown that the former effect
472   compensates for the latter effect, having an overall increase in nucleation and growth rates at lower
473   temperatures (Stolzenburg et al., 2018;Simon et al., 2020;Ye et al., 2019). While these mechanisms are clear
474   in chamber studies, the situation becomes more complicated in the atmosphere because of the complexity of
475   the atmosphere-biosphere system having simultaneous temperature-dependent processes that can enhance or
476   suppress NPF, making current atmospheric observations inconsistent on the role of temperature on NPF
477   (Kerminen et al., 2018). Solar radiation is regarded as one of the most important factors affecting NPF (Jokinen
478   et al., 2017). Its intensity is relatively high in Cyprus all year round. Intra-monthly, NPF events occurred at
479   higher global radiation during the winter and autumn month, whereas in spring (except April) and summer
480   months, radiation did not seem to be a limiting factor for NPF (Figure 11b). Inter-monthly, the month with the
481   highest solar radiation did not coincide with the highest occurrence of NPF. Regarding ambient relative
482   humidity (RH), NPF events tend to occur at lower RH in both clean and polluted environments (Kerminen et
483   al., 2018). However, high RH values do not necessarily suppress NPF (Salma and Németh, 2019), which agrees
484   with our observations (Figure 11c). In terms of the surface air pressure, intra-monthly NPF was on average
485   observed on days with higher pressures and the inter-monthly NPF occurrence was the lowest during the month
486   with the lowest surface pressure (Figure 11d). NPF occurred largely at lower wind speeds and local north-
487   easterly winds, which is the direction where the main agglomerations and livestock farming lands are situated
488   (Figure 11e, 11f & S11).

489   The EMME region is among the regions with the highest background of trace gases and aerosols concentrations
490   in the Northern Hemisphere (Lelieveld et al., 2002). Here, we investigate the relation between trace gases and
491   the occurrence of NPF (Figure 12). The intra-monthly SO_2 concentration was, on average, higher during NPF
492   event days in comparison to non-event days during most of the months. The inter-monthly SO_2 concentrations
493   during the highest NPF occurrence (Mar-May) were similar to the months with the lowest NPF occurrence
494   (Jun-Aug). This indicates that SO_2 and thus sulfuric acid (as will be shown subsequently) cannot explain the
495   seasonal pattern of NPF. The ozone (O_3) concentration is particularly high in Cyprus and is mainly influenced

496 by regional and transported ozone, while local precursor emissions play a minor role in ozone formation
497 (Kleanthous et al., 2014). Intra-monthly, the O_3 concentration was sometimes lower, similar or higher during
498 NPF event days compared with non-event days, with no clear seasonality. One notable remark is that in April,
499 NPF events took place at much higher O_3 concentrations than what was observed on non-event days. This
500 could imply that higher oxidative capacity was driving NPF during April. April also had the most notable
501 differences in global radiation and RH between NPF event and non-event days. Analogous to SO_2, O_3 cannot
502 explain the seasonal pattern of NPF. CO levels are generally high over the Mediterranean (in comparison to
503 the Pacific), with emission sources being typically from western and eastern Europe, having lower contribution
504 from the regions surrounding the Mediterranean (Lelieveld et al., 2002). The CO - NPF relationship at CAO
505 did not have a distinct character, however CO concentrations were slightly lower during the summer months.
506 Regarding NO_x, NPF event days had on average higher NO_x concentrations within the boundaries of each
507 month, except in April. More notably, NO_x had lower concentrations during the months with lower NPF
508 frequencies, which might indicate the role of associated anthropogenic organic vapors in triggering NPF at our
509 site.

510 We examined the effect of air mass origin arriving at CAO at 8:00 a.m. during event and non-event days from
511 six source regions: local, N. Africa, marine, Europe, Asia, NW. Asia, and SW. Asia (Figure 13). The last two
512 source regions represent the geographic location with respect to Cyprus location. An obvious feature that pops
513 out is that the month with the highest NPF frequency had air masses originating from south-west Asia (the
514 Middle East), whereas during the month with the lowest NPF frequency air masses did not originate from that
515 direction. This pattern might suggest that chemical compounds important for nucleation and subsequent growth
516 are transported to CAO from the Middle East. Between the end of spring and late September, which are the
517 months with the lowest NPF frequency, the circulation over the eastern Mediterranean is characterized by
518 persistent northerly winds called the Etesians (Tyrlis and Lelieveld, 2013). The NPF events during this period,
519 as shown in Sect. 3.2, were weak or did not lead to particle growth into large sizes in comparison to the rest of
520 the year. The Etesian circulation flow is caused by a sharp surface pressure difference between the westerly
521 Azorean high-pressure regime and the Asian monsoon low-pressure regime. While the Etesians block the
522 north-ward transport of desert dust, they trigger high sea levels, prevent rain over the region, and enhance
523 marine inversions (Ulbrich et al., 2012). They favor the transport of air pollutants from Central/Eastern Europe
524 and west Turkey and, together with enhanced photochemical conditions and low precipitation, contribute to
525 high O_3 (Solomou et al., 2018) and particulate matter (PM) levels (Pikridas et al., 2018). The increase in PM
526 levels during these months could be a limiting factor for NPF. Indeed, accumulation mode particles and thus
527 CS were the highest during the summer (except for July). We did not have particle size distribution
528 measurements above 700 nm, therefore bigger particles could be additionally contributing to the CS. However,
529 from mass concentration point of view, $PM_{2.5}$ and PM_{10} did not show a pattern that would support this
530 hypothesis (Figure S12 & S13). Additionally, while the south-west Asia sector might be important for NPF, it
531 did not exhibit a clear pattern during the month with the highest NPF frequency. In fact, in April most of the
532 air masses originated from north-west Asia. This sector appears to be also important for NPF during Jun, July
533 and November, whereas the other sectors did not exhibit any notable pattern.

534 Last, we investigated the relationship between sulfuric acid and formation rates. While sulfuric acid (H_2SO_4)
535 is the main nucleating species in the atmosphere, it is well known that H_2SO_4 binary nucleation with water
536 requires high H_2SO_4 vapor concentrations that are not relevant within the lower parts of the troposphere
537 (Wyslouzil et al., 1991). Additional species are required to stabilize H_2SO_4 clusters, such as ammonia, amines
538 or ions, while some other compounds can nucleate on their own in atmospherically relevant conditions,
539 including iodine oxides and highly oxygenated organic compounds (HOM) from biogenic precursors (Lee et
540 al., 2019 and references therein). In this study, the hourly H_2SO_4 proxy concentrations ranged between 3×10^5
541 and 1×10^7 cm^{-3} which are typical values for H_2SO_4 in the troposphere. The relationship between particle

542   formation rates ($J_{1.5}$) and H$_2$SO$_4$ proxy concentration varied across the month of the year (Figure 14). Lower
543   concentrations of H$_2$SO$_4$ were required during winter and spring to achieve the same formation rates as in the
544   other seasons. A possible explanation to this behavior is that in the first case, stabilizing compounds are
545   abundant in the atmosphere and thus less H$_2$SO$_4$ is required for the formation of particles. A similar hypothesis
546   was tested by Pikridas et al. (2012) by using the accumulation mode particle acidity as an indirect measure of
547   the availability or lack of ammonia or any other basic species in the gas phase. The authors concluded that
548   excess base is not available during the summer to participate in the nucleation process. In our case, however,
549   the formation rate versus H$_2$SO$_4$ relationship is closer to those derived for the H$_2$SO$_4$-DMA-NH$_3$-H$_2$O system
550   than those for the H$_2$SO$_4$-NH$_3$-H$_2$O system. In fact, the ternary nucleation of H$_2$SO$_4$ -NH$_3$-H$_2$O is unlikely to
551   be important at ground level either because of too low concentrations or too high temperatures (Kürten et al.,
552   2018). This suggests that, in our case, the missing stabilizing base is probably not ammonia. The distinct air
553   mass origin during the summer could explain the decrease in the concentrations of the stabilizing base.
554   Otherwise, the high temperature during the summer could be the factor that disfavors the occurrence of NPF.
555   Most certainly, NPF at CAO seem to be influenced by several factors and chemical constituents. This has been
556   also indicated by Debevec et al. (2018) whom observed four types on nucleation events, within one month of
557   measurements, having: 1) predominant anthropogenic influence, 2) predominant biogenic influence, 3) mixed
558   anthropogenic - biogenic influence, and 4) a marine influence with low concentrations of anthropogenic and
559   biogenic tracers. Therefore, to reveal the main mechanisms of NPF, long-term measurements of nucleating
560   clusters and organic precursors using state-of-the-art online mass spectrometry techniques are essential.

561   **4   Conclusion**
562   Recent studies have pointed out that NPF is important in the EMME region (Brilke et al., 2020;Debevec et al.,
563   2018;Hakala et al., 2019;Hussein et al., 2020;Kalivitis et al., 2019;Kalkavouras et al., 2019). Brilke et al.
564   (2020) studied NPF in a coastal site in Cyprus with strong local pollution during 2017, while Debevec et al.
565   (2018) characterized NPF at the same site of this study during 2015. While both studies were limited to one
566   month of observations, we disclosed here the first long-term (one year) characterization of NPF at a
567   background site in Cyprus. We presented the general and seasonal characteristics of PSD and NPF then we
568   explored the factors that affect NPF.
569   Our analysis of NPF intra-monthly variability showed that on average, NPF events occurred at higher
570   temperatures, lower RH and higher global radiation, except during the months of August, September and
571   December. To the contrary, lower pressure conditions, higher wind speeds and local northwest wind directions
572   seemed to be more favorable for non-events. The frequency of NPF was higher than that reported at a similar
573   Eastern Mediterranean island site using a slightly limited measurement setup than the one applied here. This
574   demonstrates the importance of comprehensive measurements using instruments that can measure down to
575   cluster sizes. NPF occurred all year round, with higher frequencies during the spring and autumn and a
576   minimum frequency during the summer. The particles did not grow significantly after nucleation during the
577   months with the lowest NPF frequencies. These months were also characterized by lower NO$_x$ concentrations,
578   an indication of lower anthropogenic influence, and distinct air mass origin profiles from the rest of the year.
579   Condensation sink, calculated based on PSD up to 700 nm, had no clear relationship with NPF, but it was
580   slightly higher during some summer month. Additionally, sulfuric acid was not the limiting factor for NPF
581   occurrence as its estimated concentration was mostly high during the summer, up to 1e^7 molecules.cm^{-3}.The
582   relationship between particle formation rates and sulfuric acid proxy exhibited different slopes between the
583   months with the highest and lowest NPF frequency, suggesting that nucleation might have proceeded with
584   varying temperatures or at different concentrations of stabilizing compounds and other aerosol precursors not
585   measured in this study.
586   The analysis presented in this study is a step forward towards understanding the mechanisms of NPF
587   mechanism in the EMME region. Future studies require long-term measurements of vapors that participate in
588   NPF and subsequent growth. These could include, for example, ultra-low volatility organic compounds

589   (ULVOC), extremely low-volatility organic compounds (ELVOC), low-volatility organic compounds
590   (LVOC), ammonia, amines and iodic species. Further, to understand the ubiquity of the effect of large particles
591   which could inhibit NPF during certain episodes but enhance NPF during episodes with high mineral dust
592   loadings, extended PSD measurements up to coarse particles, preferably coupled with chemical speciation, are
593   important. On a larger scale, long-term measurements of CCN particles are necessary to quantify the
594   contribution of NPF to the CCN budget. These measurements would preferably take place not only in Cyprus
595   but also in different location in the Middle East and North Africa.

Atmospheric
Chemistry
and Physics
Discussions

596 **Data availability**
597 Data used in this study are available from the corresponding author upon request (rima.baalbaki@helsinki.fi)

598 **Author Contributions**
599 The study was conceived by MK and JS. RB, TJ, TL, KN and MP prepared and installed the instruments. RB,
600 MP, KN, AM, EB, AC, and FU performed the regular maintenance for the instruments. RB performed the data
601 analysis and wrote the manuscript. LD provided support in data analysis. LA provided support in instrument
602 troubleshooting and nCNC inversion. MP and EB performed the sector analysis. SB performed the kappa
603 measurements and provided support on hygroscopisity calculations. MP and JS provided the SMPS data. CS
604 provided the meteorological and trace gas data. RB, MP, TJ, LD, SB, KL, JK, GB, TP, VMK, and MK
605 participated in the scientific discussion and reviewed the manuscript.

606 **Competing interests**
607 The authors declare no conflict of interest.

Table 1. Monthly values of observed formation rates (cm^{-3} s^{-1}) during NPF events (calculated within the event duration using daily data). The maximum values and minimum values of the mean and median are highlighted.

		Jan	Feb	Mar	Apr	May	Jun	Jul	Aug	Sep	Oct	Nov	Dec	All
J$_{1.5}$ **(cm^{-3}.s^{-1})**	Mean	6.43	17.81	19.98	**39.71**	6.78	na	4.50	10.36	10.29	5.61	8.15	na	16.18
	SD	2.94	24.77	14.84	93.97	6.39	na	3.00	10.60	10.77	6.28	na	na	41.82
	25th	4.28	6.18	6.13	5.82	3.35	na	1.99	3.26	1.01	0.95	na	na	3.74
	Median	6.83	10.19	**18.52**	12.46	4.46	na	4.07	6.97	8.99	3.53	8.15	na	7.87
	75th	8.39	16.96	29.71	34.11	6.92	na	7.32	13.84	14.23	9.09	na	na	16.01
	90th	10.18	34.28	42.52	69.59	17.61	na	8.30	27.07	23.60	12.34	na	na	35.26
	N	5	16	21	23	17	na	9	10	13	18	1	na	133
J$_{3}$ **(cm^{-3}.s^{-1})**	Mean	1.57	4.68	5.65	**8.77**	3.00	3.48	5.03	3.85	5.53	3.00	2.42	na	4.97
	SD	0.91	3.44	4.65	15.74	2.48	2.60	6.57	4.19	5.58	5.16	na	na	7.79
	25th	0.81	2.31	1.96	1.98	0.88	0.98	0.82	0.93	0.38	0.31	na	na	0.99
	Median	1.16	4.16	3.81	**4.14**	2.04	3.32	2.23	1.72	4.93	1.11	2.42	na	2.69
	75th	2.54	5.93	7.72	8.88	4.45	6.23	5.88	7.83	10.06	2.42	na	na	6.42
	90th	2.56	9.30	13.00	11.44	6.46	6.57	18.15	10.65	12.46	8.98	na	na	11.17
	N	5	16	21	26	20	6	13	11	14	19	1	na	152
J$_{7}$ **(cm^{-3}.s^{-1})**	Mean	0.58	**1.53**	1.17	1.51	1.30	0.45	1.59	0.49	1.32	0.71	1.15	na	1.18
	SD	0.51	1.17	1.09	1.91	1.44	0.34	2.20	0.72	1.75	0.59	na	na	1.43
	25th	0.19	0.35	0.26	0.35	0.20	0.26	0.09	0.09	0.08	0.17	na	na	0.22
	Median	0.29	**1.57**	0.78	0.83	0.57	0.36	0.38	0.35	0.59	0.39	1.15	na	0.61
	75th	1.08	2.13	1.70	2.04	2.41	0.55	2.71	0.56	1.69	1.37	na	na	1.57
	90th	1.25	2.72	2.82	3.33	3.72	1.02	5.52	1.41	3.48	1.50	na	na	3.04
	N	5	16	21	26	20	6	13	11	14	19	1	na	152

Table 2. Comparison of formation rates and growth rates from long-term measurements at various sites including this study

Site	Type	Period	J_3			GR_{3-25}			Reference
			Mean±SD	Median	Min-max	Mean±SD	Median	Min-max	
CAO, Cyprus	Rural	2018	4.97±7.79	2.69	0.04-78.85	7.94±5.35	6.25	2.31-31.9	This study
Vavihill, Sweden	Rural	2001-2004	4.3	1.89		2.5	2.1		(Kristensson et al., 2008)
Hyytiälä, Finland	Rural	1996-2004	0.8	0.6	0.06–5.0	3.0	2.5	0.5-15.1	(Dal Maso et al., 2007)
Värriö, Finland	Rural	1996-2004	0.2	0.1		2.7	2.4	0.8–9.7	(Dal Maso et al., 2007)
Tomsk, Russia	Rural	2005-2006	0.4	0.4	0.04-1.1	5.5	3.5	2.6-23	(Dal Maso et al., 2008)
Beijing, China	Urban clean Urban polluted	2004-2005	22.3±15.1 16.2±12	18.7 9.9	4.4-81.4 3.3-51.7	1.8±2 4.4±3.2	1.1 3.9	0.1-7.9 0.3-11.2	(Wu et al., 2007)
St. Louis, U.S.	Urban	2001-2003	17±20	9		5.9±4.7	4.7		(Qian et al., 2007)
Po Valley, Italy	Rural w. urban influence	2002-2005	5.89	3.31	0.24-36.89	6.82	6.45	2.9-22.9	(Hamed et al., 2007)
Budapest, Hungary	Urban	2008-2009	4.2±2.5 [a]	4.2 [a]	1.65-12.5 [a]	7.7±2.4 [a]	7.7 [a]	2-17.3 [a]	(Salma et al., 2011)
Helsinki, Finland	Urban	1997-2006	2 [b]	1.09[b]	0.63-2.87 [b]	3.39[b]	2.85 [b]	2.21-6.55 [b]	(Hussein et al., 2008)
Zeppelin, Norway	Arctic	2016-2018			0.02-1.62			0.35-7.55	(Lee et al., 2020)
Finokalia, Greece	Remote coastal	2008-2009				7.5±5.8[c]			(Pikridas et al., 2012)

[a] data represent 6-25 nm range

[b] calculated from monthly values

[c] GR for 7-20nm

Table 3. Monthly values of the observed growth rates (nm.h^{-1}) computed mainly during class I events or when possible.

		Jan	Feb	Mar	Apr	May	Jun	Jul	Aug	Sep	Oct	Nov	Dec	All
GR (1.5 – 3 nm)	**Mean**	1.17	1.74	3.19	2.80	3.55	1.70	5.22	4.20	4.26	1.80	3.94	5.70	3.01
	SD	0.87	0.96	2.13	1.71	2.54	na	5.37	3.74	3.47	1.05	3.04	2.07	2.44
	25th	0.68	1.00	1.42	1.57	2.02	na	1.43	1.93	1.79	1.23	1.17	4.52	1.27
	Median	1.08	1.05	2.42	2.12	3.05	1.70	5.22	2.66	2.09	1.62	3.26	5.43	2.04
	75th	1.87	2.46	4.46	3.95	5.09	na	9.02	6.47	7.83	1.80	7.10	6.43	4.25
	90th	2.37	3.11	6.52	5.70	7.08	na	9.02	9.73	8.94	3.46	7.17	9.14	7.10
	N	9	7	10	10	4	1	2	4	7	9	5	5	73
GR (3-7 nm)	**Mean**	4.40	7.13	6.76	4.52	5.23	10.88	7.46	4.11	10.56	5.28	6.18	5.68	6.21
	SD	3.44	6.19	3.75	1.94	1.17	na	3.01	2.16	8.82	3.26	5.15	3.60	4.58
	25th	2.45	3.48	3.78	3.23	4.66	na	5.64	2.30	2.31	3.55	2.80	3.01	3.25
	Median	4.03	4.61	5.92	4.22	5.71	10.88	7.53	3.90	6.81	4.80	3.21	4.64	4.84
	75th	6.73	6.79	8.63	5.35	5.89	na	8.89	5.93	17.19	5.71	8.66	7.67	6.83
	90th	9.46	18.26	13.43	6.25	6.24	na	11.96	6.56	23.10	9.17	15.04	11.57	12.94
	N	9	10	16	14	6	1	5	4	9	12	9	5	100
GR (7 –20 nm)	**Mean**	7.11	21.13	8.67	7.74	11.20	5.94	20.32	13.03	10.77	7.24	7.00	8.06	10.60
	SD	8.30	16.34	5.28	3.39	8.02	na	15.62	14.36	5.29	2.72	5.89	4.08	9.45
	25th	2.35	7.39	5.01	6.58	4.94	na	7.73	4.96	7.06	5.76	2.70	4.38	5.40
	Median	5.14	22.10	6.39	7.09	8.25	5.94	16.64	7.17	10.45	6.95	5.40	8.11	7.40
	75th	7.88	26.21	10.48	10.70	17.26	na	25.54	21.10	15.11	9.04	8.65	11.65	12.58
	90th	21.05	45.83	19.40	12.77	23.54	na	45.95	34.38	17.85	10.64	16.30	12.81	22.44
	N	8	11	15	14	8	1	6	4	8	12	9	6	102
GR (3 –25 nm)	**Mean**	5.98	13.96	8.88	6.21	7.80	5.66	12.11	5.65	7.37	5.89	5.69	7.63	7.94
	SD	1.49	10.74	5.27	2.43	3.88	na	4.66	1.90	3.69	2.29	2.97	2.19	5.35
	25th	5.14	5.10	5.37	4.67	5.06	na	9.15	4.05	4.51	4.32	3.03	5.47	4.68
	Median	6.08	9.45	7.27	5.67	6.57	5.66	9.99	5.43	6.27	5.12	5.51	8.74	6.25
	75th	7.05	23.91	10.38	6.62	10.94	na	16.84	7.25	9.95	6.78	8.93	9.38	9.31
	90th	7.63	30.81	18.28	10.63	13.85	na	17.24	7.78	13.09	9.78	9.60	9.55	13.96
	N	6	11	13	14	7	1	5	4	8	12	9	5	95

Figure 1. Maps of the Mediterranean region and Cyprus. (a) Location of Cyprus in the Mediterranean region. (b) Location of the measurement site (CAO) in Cyprus. (c) Location of the measurement site (CAO) pointed by the blue location marker with respect to the villages of Agia Marina and Xyliatos. The geographic border of the villages is marked by the yellow enclosure. The maps were retrieved from Google (©2020 Google, TerraMetrics).
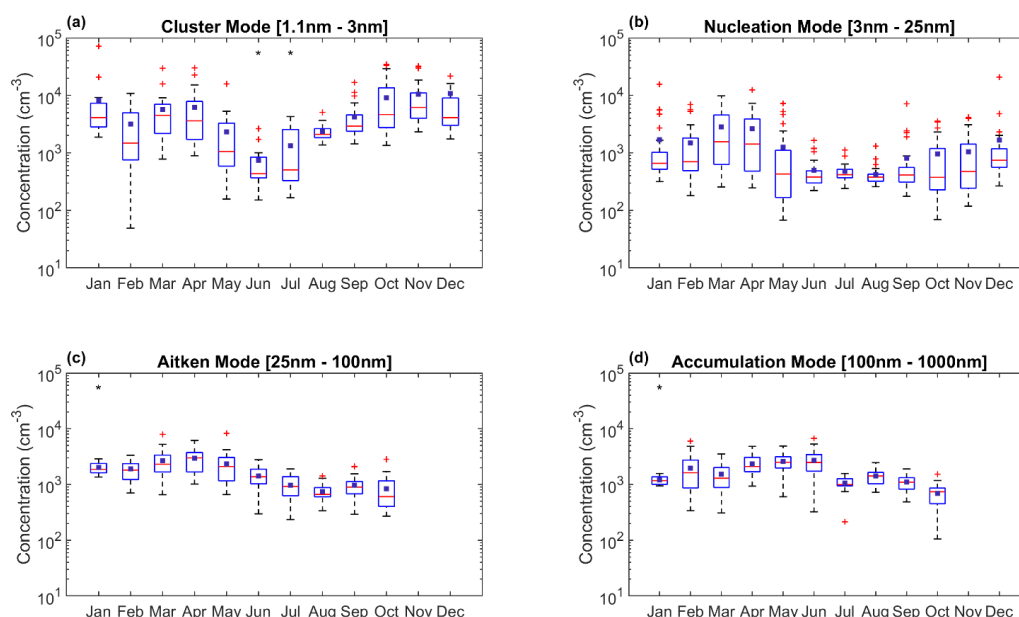
Figure 2. Monthly variation (at radiation >50 W. m^{-2}) of particle number concentration of (a) cluster mode, (b) nucleation mode, (c) Aitken mode, and (d) accumulation mode presented by box plots. The central red marks indicate the median, the blue small boxes indicate the mean, the bottom and top edges of the big box indicate the 25th and 75th percentiles, respectively. The whiskers extend to the most extreme data points not considered outliers, and the outliers are plotted individually using the '+' symbol. Data presented have daily time resolution. Month designated with '*' symbol have less than 20 days of data. Note that SMPS measurements were not available on November and December.
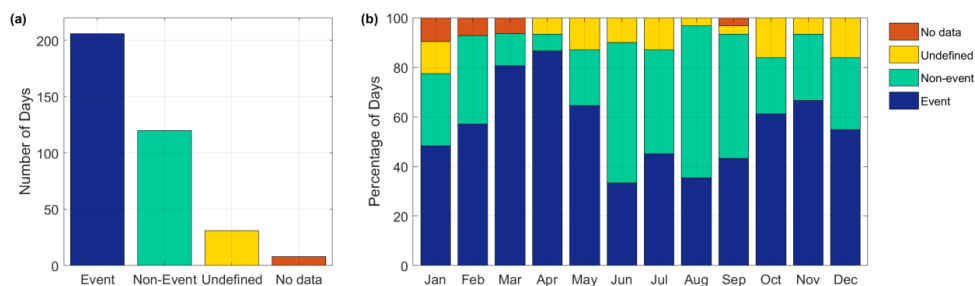
Figure 3. Classification of NPF events presented (a) annually and (b) seasonally.
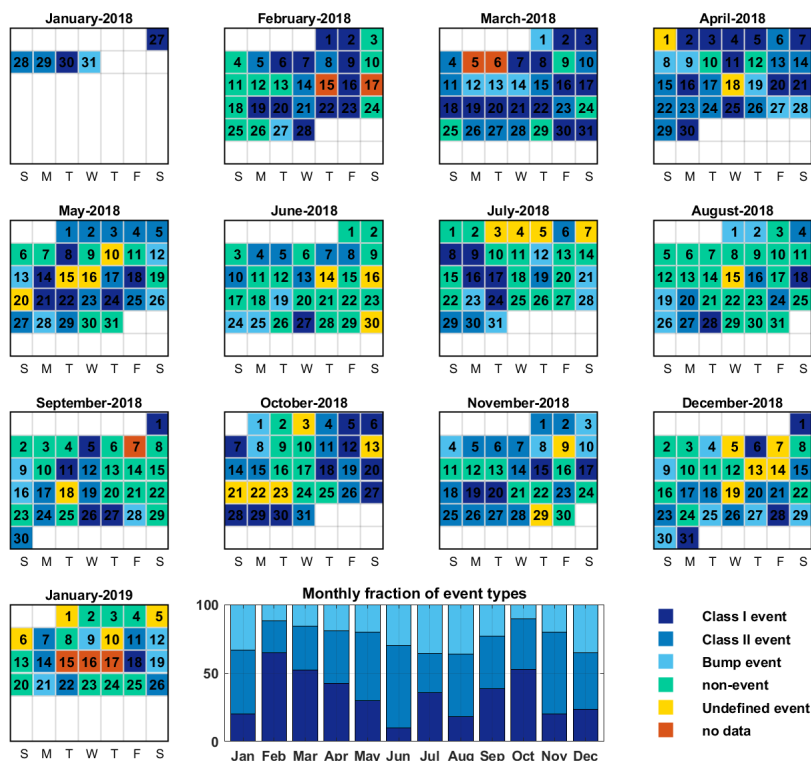
Figure 4. Calendar of daily event day classification between January 27, 2018 –January 26, 2019 and the monthly fraction of NPF event classes.
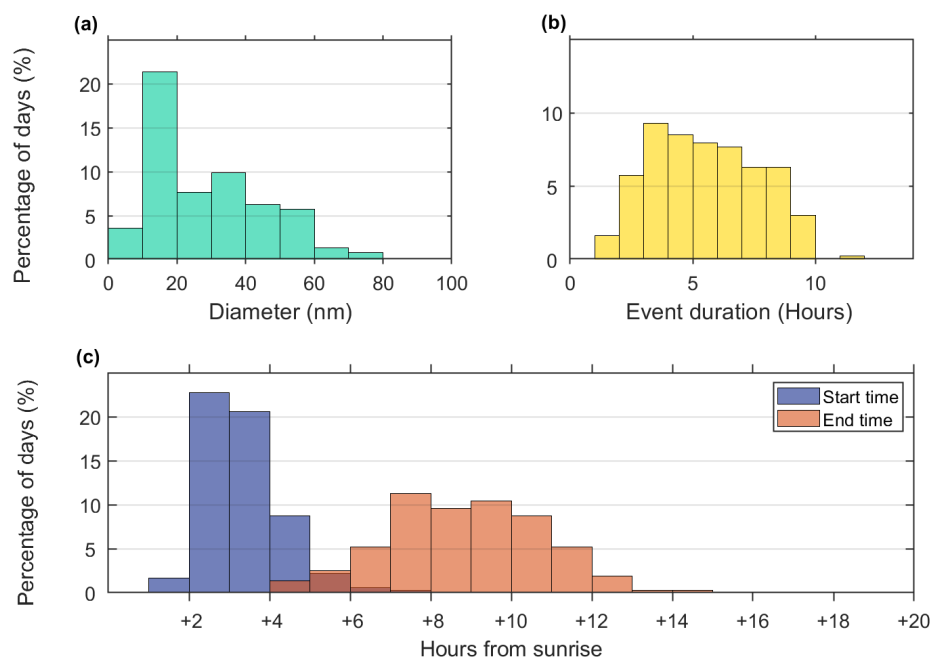
Figure 5. Percentage histograms showing the frequency distribution of (a) NPF events growing to a certain diameter, (b) NPF event duration, and (c) the event start and end times from sunrise.
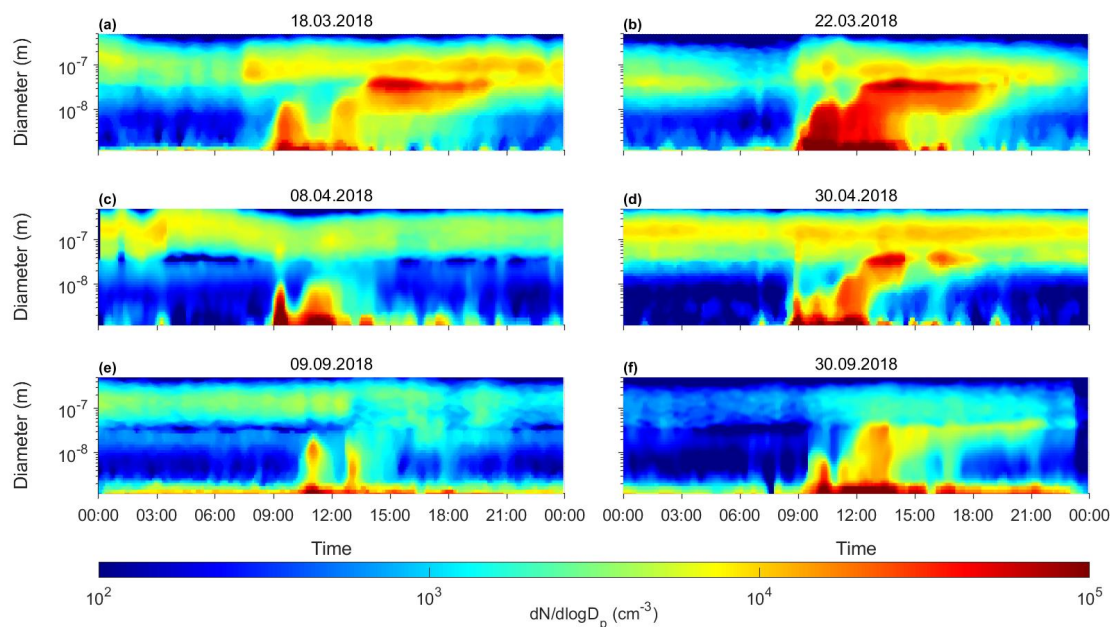
Figure 6. Examples of days with multiple nucleation events: (a) March 18, 2018 (b) March 22, 2018 (c) April 8, 2019, (d) April 30, 2018, (e) September 9, 2018 and (f) September 30, 2018.
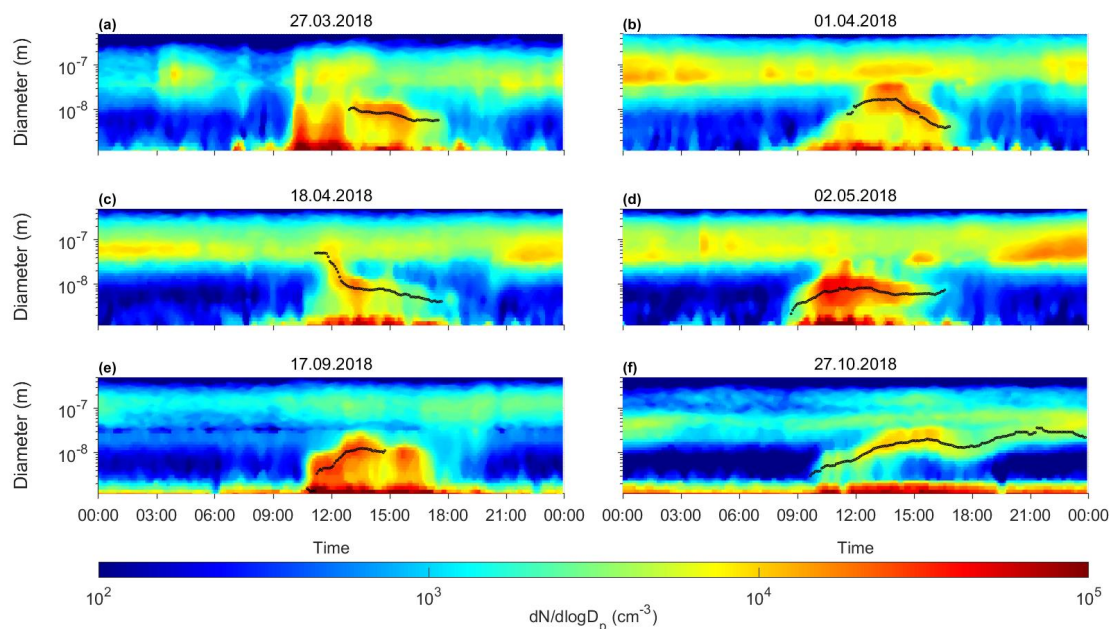
Figure 7. Example of days showing a decreasing mode diameter: (a) March 27, 2018, (b) April 1, 2018, (c) April 18, 2018, (d) May 2, 2018, (e) September 17, 2018 and (f) October 27, 2018 in local time. The mode diameter is plotted as black circular markers.
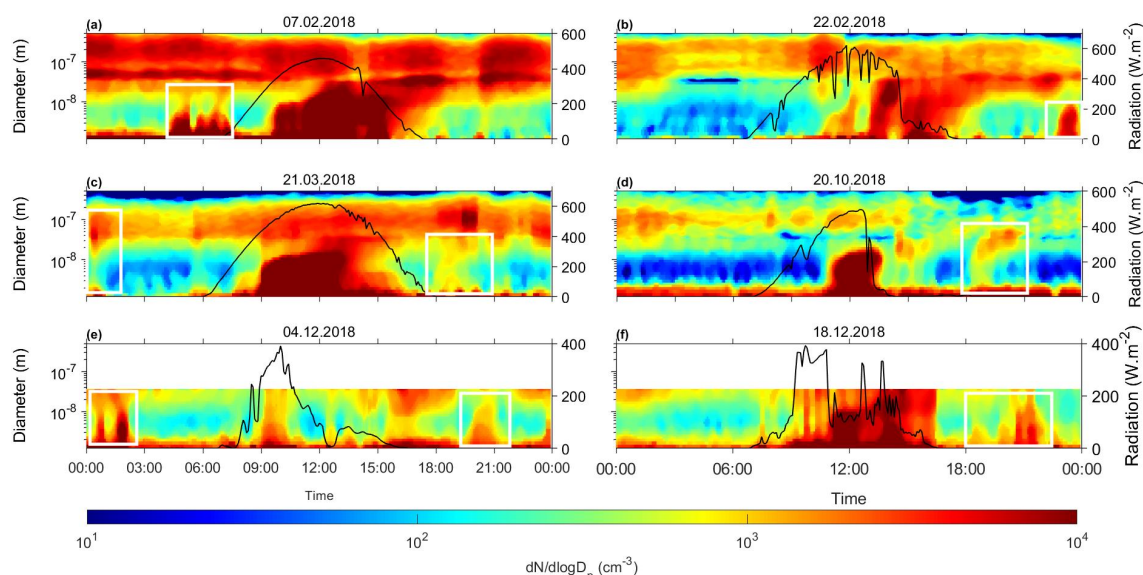
Figure 8. Examples of days with nighttime clustering and growth marked with white rectangles: (a) February 7, 2018, (b) February 22, 2018, (c) March 21, 2018, (d) October 20, 2018, (e) December 04, 2018 and (f) December 18, 2018. The black line is the solar radiation (W.m^{-2}) which can be read from the right axis. Note the difference in the color scale used in this figure in comparison to figures 6 and 7.
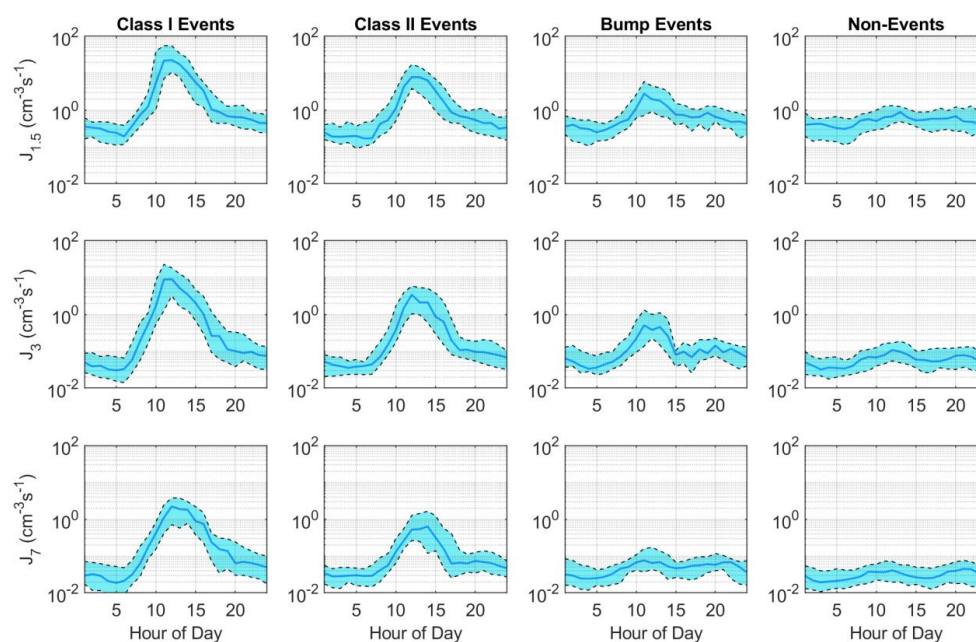
Figure 9. Diurnal variation of J1.5 (top), J3 (middle) and J7 (bottom) during class I, class II, bump events and non-events. Shaded areas represent the 25th and 75th percentile bounds while the solid line represents the median.
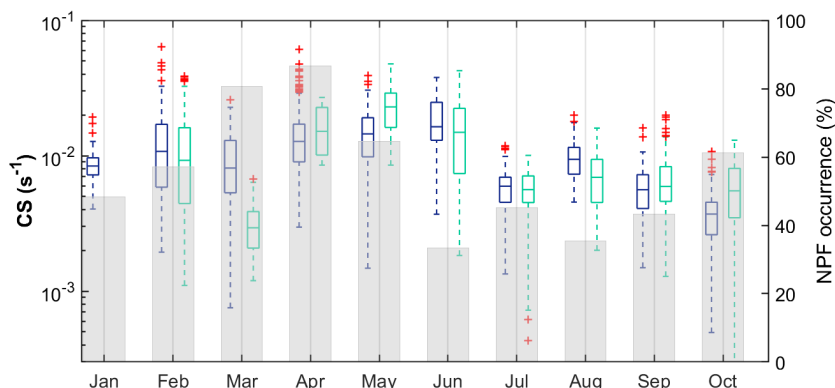
Figure 10. Monthly variation of condensation sink (s^{-1}) during event (blue) and non-event (green) days using data corresponding to global radiation is greater than 50 W.m^{-2}. The bottom and top edges of the box plots indicate the 25th and 75th percentiles, respectively. The central mark indicates the median. The whiskers extend to the most extreme data points not considered outliers, and the outliers are plotted individually using the '+' symbol. Data presented have hourly time resolution. The shaded grey bars represent the monthly NPF percent occurrence
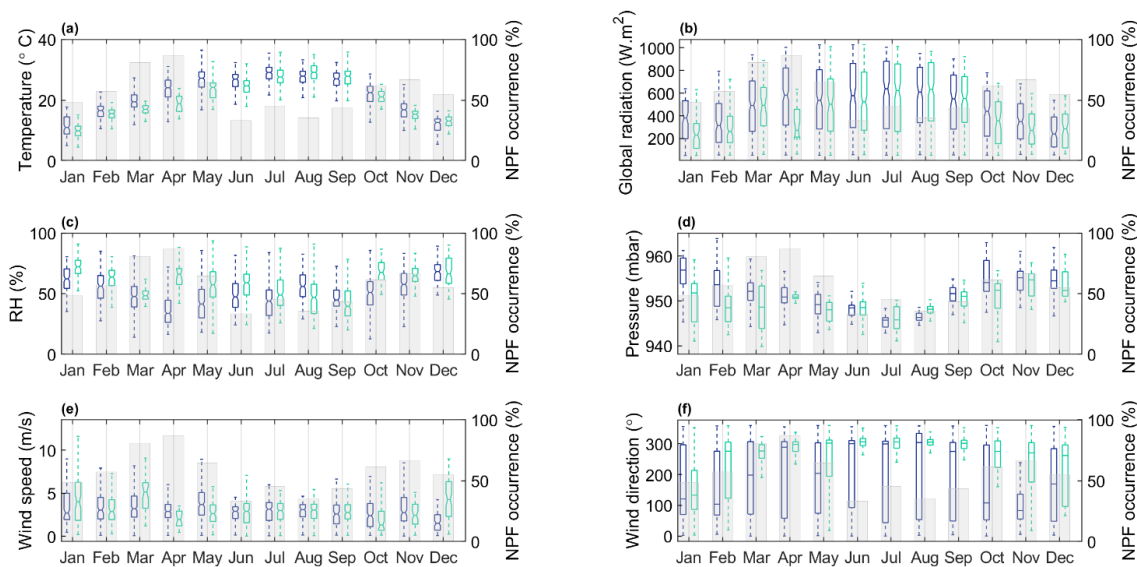
Figure 11. Monthly variation of metrological parameters during event (blue) and non-event (green) days: (a) temperature, (b) global radiation, (c) relative humidity, (d) pressure, (e) wind speed, and (f) wind direction using data corresponding to global radiation is greater than 50 W.m^{-2}. The bottom and top edges of the box plots indicate the 25th and 75th percentiles, respectively. The central mark indicates the median. The whiskers extend to the extreme data points not considered outliers. Data presented have hourly time resolution. The shaded grey bars represent the monthly NPF percent occurrence
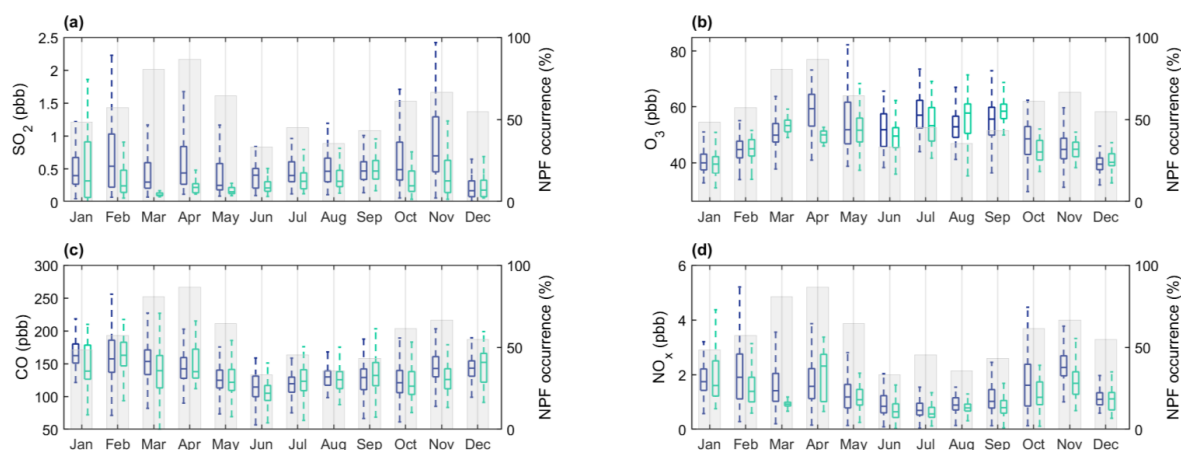
Figure 12. Monthly variation of trace gases during event (blue) and non-event (green) days: (a) sulfur dioxide, (b) ozone, (c) carbon monoxide, and (d) nitrogen oxide using data corresponding to global radiation is greater than 50 W.m^{-2}. The shaded grey bars represent the monthly NPF percent occurrence. The bottom and top edges of the box plots indicate the 25th and 75th percentiles, respectively. The central mark indicates the median. The whiskers extend to the most extreme data points not considered outliers. Data presented have hourly time resolution.
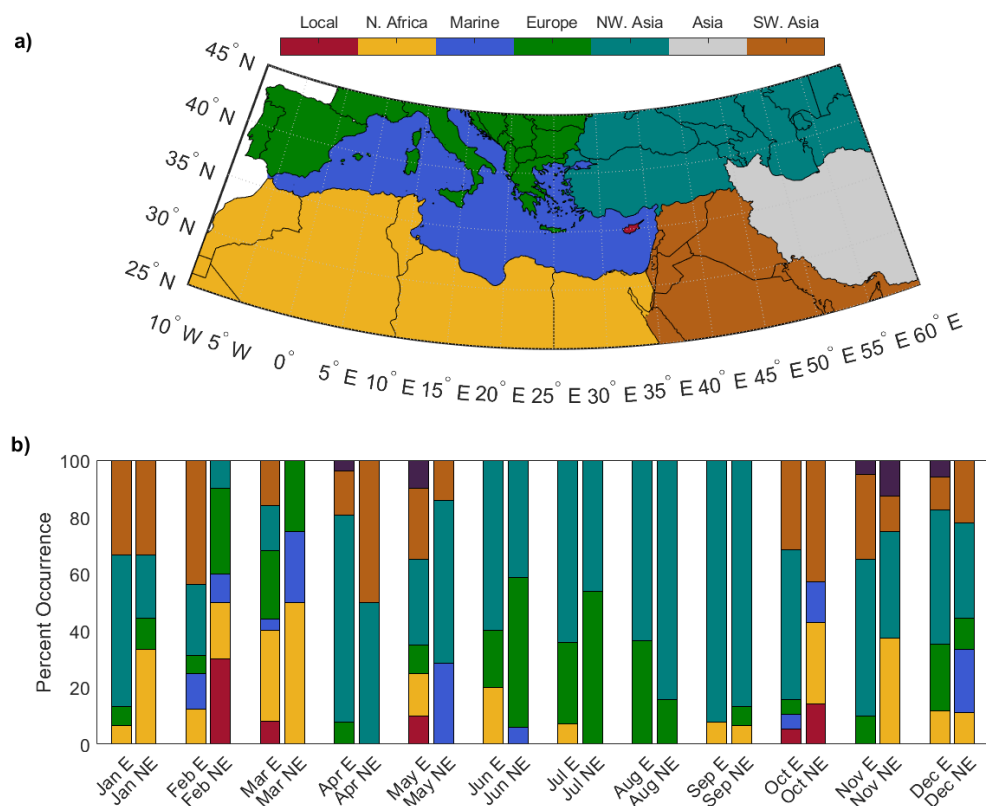
Figure 13. a) The source regions of air masses reaching CAO used for the air mass sector analysis. The map was plotted using The Climate Data Toolbox for MATLAB (Greene et al., 2019). The IHO World Sea Areas v3 were used to retrieve the boundaries of the Mediterranean Sea (Flanders Marine Institute, 2019). Note that marine areas other than the Mediterranean Sea were considered part of the continental sectors and that the NW. Asia and SW. Asia sectors are with respect to Cyprus location. b) Monthly variation of air mass origin arriving at CAO at 8:00 a.m. during event (E) and non-event days (NE). There are no air masses originating from Asia sector because those are obscured by terrain height.
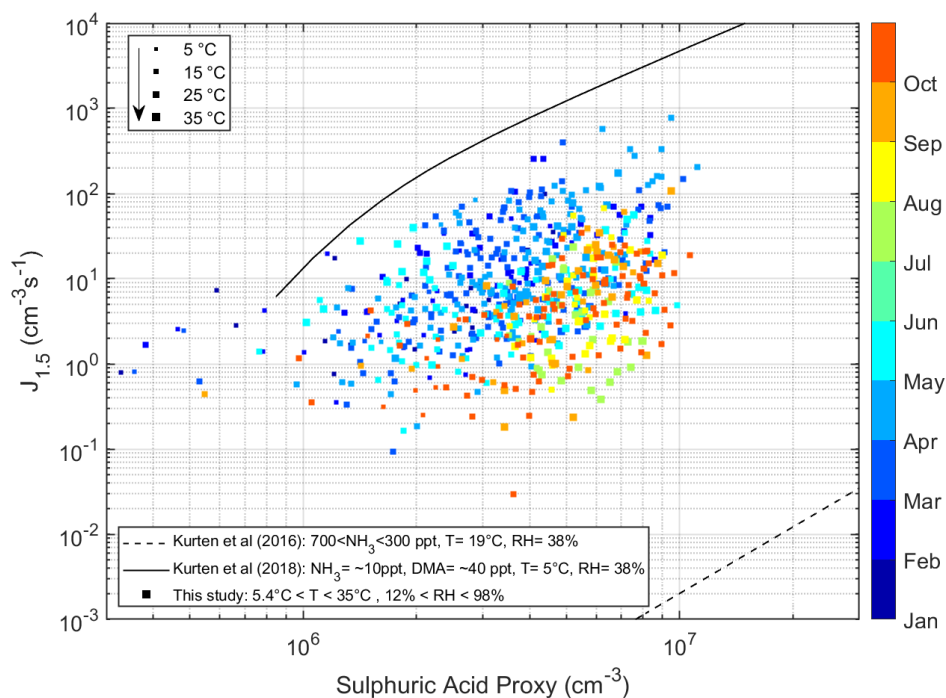
Figure 14. $J_{1.5}$ versus sulfuric acid proxy concentrations color-coded by the month of the year. Data presented have hourly time resolution.

References

Achilleos, S., Evans, J. S., Yiallouros, P. K., Kleanthous, S., Schwartz, J., and Koutrakis, P.: PM10 concentration levels at an urban and background site in Cyprus: The impact of urban sources and dust storms, Journal of the Air & Waste Management Association, 64, 1352-1360, https://doi.org/10.1080/10962247.2014.923061, 2014.

Alonso-Blanco, E., Gómez-Moreno, F. J., Núñez, L., Pujadas, M., Cusack, M., and Artíñano, B.: Aerosol particle shrinkage event phenomenology in a South European suburban area during 2009–2015, Atmospheric Environment, 160, 154-164, https://doi.org/10.1016/j.atmosenv.2017.04.013, 2017.

Baccarini, A., Karlsson, L., Dommen, J., Duplessis, P., Vüllers, J., Brooks, I. M., Saiz-Lopez, A., Salter, M., Tjernström, M., Baltensperger, U., Zieger, P., and Schmale, J.: Frequent new particle formation over the high Arctic pack ice by enhanced iodine emissions, Nature Communications, 11, 4924, https://doi.org/10.1038/s41467-020-18551-0, 2020.

Backman, J., Rizzo, L. V., Hakala, J., Nieminen, T., Manninen, H. E., Morais, F., Aalto, P. P., Siivola, E., Carbone, S., Hillamo, R., Artaxo, P., Virkkula, A., Petäjä, T., and Kulmala, M.: On the diurnal cycle of urban aerosols, black carbon and the occurrence of new particle formation events in springtime São Paulo, Brazil, Atmos. Chem. Phys., 12, 11733-11751, https://doi.org/10.5194/acp-12-11733-2012, 2012.

Berland, K., Rose, C., Pey, J., Culot, A., Freney, E., Kalivitis, N., Kouvarakis, G., Cerro, J. C., Mallet, M., Sartelet, K., Beckmann, M., Bourriane, T., Roberts, G., Marchand, N., Mihalopoulos, N., and Sellegri, K.: Spatial extent of new particle formation events over the Mediterranean Basin from multiple ground-based and airborne measurements, Atmos. Chem. Phys., 17, 9567-9583, https://doi.org/10.5194/acp-17-9567-2017, 2017.

Bianchi, F., Tröstl, J., Junninen, H., Frege, C., Henne, S., Hoyle, C. R., Molteni, U., Herrmann, E., Adamov, A., Bukowiecki, N., Chen, X., Duplissy, J., Gysel, M., Hutterli, M., Kangasluoma, J., Kontkanen, J., Kürten, A., Manninen, H. E., Münch, S., Peräkylä, O., Petäjä, T., Rondo, L., Williamson, C., Weingartner, E., Curtius, J., Worsnop, D. R., Kulmala, M., Dommen, J., and Baltensperger, U.: New particle formation in the free troposphere: A question of chemistry and timing, Science, 352, 1109-1112, https://doi.org/10.1126/science.aad5456 %J Science, 2016.

Bianchi, F., Kurtén, T., Riva, M., Mohr, C., Rissanen, M. P., Roldin, P., Berndt, T., Crounse, J. D., Wennberg, P. O., Mentel, T. F., Wildt, J., Junninen, H., Jokinen, T., Kulmala, M., Worsnop, D. R., Thornton, J. A., Donahue, N., Kjaergaard, H. G., and Ehn, M.: Highly Oxygenated Organic Molecules (HOM) from Gas-Phase Autoxidation Involving Peroxy Radicals: A Key Contributor to Atmospheric Aerosol, Chemical Reviews, 119, 3472-3509, https://doi.org/10.1021/acs.chemrev.8b00395, 2019.

Brilke, S., Fölker, N., Müller, T., Kandler, K., Gong, X., Peischl, J., Weinzierl, B., and Winkler, P. M.: New particle formation and sub-10 nm size distribution measurements during the A-LIFE field experiment in Paphos, Cyprus, Atmospheric Chemistry and Physics, 20, 5645-5656, https://doi.org/10.5194/acp-20-5645-2020, 2020.

Brines, M., Dall'Osto, M., Beddows, D. C. S., Harrison, R. M., Gómez-Moreno, F., Núñez, L., Artíñano, B., Costabile, F., Gobbi, G. P., Salimi, F., Morawska, L., Sioutas, C., and Querol, X.: Traffic and nucleation events as main sources of ultrafine particles in high-insolation developed world cities, Atmos. Chem. Phys., 15, 5929-5945, https://doi.org/10.5194/acp-15-5929-2015, 2015.

Brockmann, J. E.: Aerosol Transport in Sampling Lines and Inlets, in: Aerosol Measurement: Principles, Techniques and Applications, Third edition ed., edited by: Pramod Kulkarni, Paul A. Baron, and Willeke, K., John Wiley & Sons, Hoboken, New Jersey, 69-105, 2011.

Cai, R., Yang, D., Ahonen, L. R., Shi, L., Korhonen, F., Ma, Y., Hao, J., Petäjä, T., Zheng, J., Kangasluoma, J., and Jiang, J.: Data inversion methods to determine sub-3 nm aerosol size distributions using the

particle size magnifier, Atmos. Meas. Tech., 11, 4477-4491, https://doi.org/10.5194/amt-11-4477-2018, 2018.

Carnerero, C., Pérez, N., Reche, C., Ealo, M., Titos, G., Lee, H. K., Eun, H. R., Park, Y. H., Dada, L., Paasonen, P., Kerminen, V. M., Mantilla, E., Escudero, M., Gómez-Moreno, F. J., Alonso-Blanco, E., Coz, E., Saiz-Lopez, A., Temime-Roussel, B., Marchand, N., Beddows, D. C. S., Harrison, R. M., Petäjä, T., Kulmala, M., Ahn, K. H., Alastuey, A., and Querol, X.: Vertical and horizontal distribution of regional new particle formation events in Madrid, Atmospheric Chemistry and Physics, 18, 16601-16618, https://doi.org/10.5194/acp-18-16601-2018, 2018.

Casquero-Vera, J. A., Lyamani, H., Dada, L., Hakala, S., Paasonen, P., Román, R., Fraile, R., Petäjä, T., Olmo-Reyes, F. J., and Alados-Arboledas, L.: New particle formation at urban and high-altitude remote sites in the south-eastern Iberian Peninsula, Atmos. Chem. Phys. Discuss., 2020, 1-32, https://doi.org/10.5194/acp-2020-394, 2020.

Chan, T., Cai, R., Ahonen, L. R., Liu, Y., Zhou, Y., Vanhanen, J., Dada, L., Chao, Y., Liu, Y., Wang, L., Kulmala, M., and Kangasluoma, J.: Assessment of particle size magnifier inversion methods to obtain particle size distribution from atmospheric measurements, Atmos. Meas. Tech. Discuss., 2020, 1-21, https://doi.org/10.5194/amt-2019-465, 2020.

Chen, X., Virkkula, A., Kerminen, V. M., Manninen, H. E., Busetto, M., Lanconelli, C., Lupi, A., Vitale, V., Del Guasta, M., Grigioni, P., Väänänen, R., Duplissy, E. M., Petäjä, T., and Kulmala, M.: Features in air ions measured by an air ion spectrometer (AIS) at Dome C, Atmos. Chem. Phys., 17, 13783-13800, https://doi.org/10.5194/acp-17-13783-2017, 2017.

Chu, B., Kerminen, V. M., Bianchi, F., Yan, C., Petäjä, T., and Kulmala, M.: Atmospheric new particle formation in China, Atmospheric Chemistry and Physics, 19, 115-138, https://doi.org/10.5194/acp-19-115-2019, 2019.

Cusack, M., Alastuey, A., and Querol, X.: Case studies of new particle formation and evaporation processes in the western Mediterranean regional background, Atmospheric Environment, 81, 651-659, https://doi.org/10.1016/j.atmosenv.2013.09.025, 2013.

Dada, L., Paasonen, P., Nieminen, T., Buenrostro Mazon, S., Kontkanen, J., Peräkylä, O., Lehtipalo, K., Hussein, T., Petäjä, T., Kerminen, V. M., Bäck, J., and Kulmala, M.: Long-term analysis of clear-sky new particle formation events and nonevents in Hyytiälä, Atmospheric Chemistry and Physics, 17, 6227-6241, https://doi.org/10.5194/acp-17-6227-2017, 2017.

Dada, L., Chellapermal, R., Buenrostro Mazon, S., Paasonen, P., Lampilahti, J., Manninen, H. E., Junninen, H., Petäjä, T., Kerminen, V. M., and Kulmala, M.: Refined classification and characterization of atmospheric new-particle formation events using air ions, Atmospheric Chemistry and Physics, 18, 17883-17893, https://doi.org/10.5194/acp-18-17883-2018, 2018.

Dada, L., Ylivinkka, I., Baalbaki, R., Li, C., Guo, Y., Yan, C., Yao, L., Sarnela, N., Jokinen, T., Daellenbach, K. R., Yin, R., Deng, C., Chu, B., Nieminen, T., Kontkanen, J., Stolzenburg, D., Sipilä, M., Hussein, T., Paasonen, P., Bianchi, F., Salma, I., Weidinger, T., Pikridas, M., Sciare, J., Jiang, J., Liu, Y., Petäjä, T., Kerminen, V. M., and Kulmala, M.: Sources and sinks driving sulphuric acid concentrations in contrasting environments: implications on proxy calculations, Atmospheric Chemistry Physics Discussion., 2020, 1-24, https://doi.org/10.5194/acp-2020-155, 2020.

Dai, L., Wang, H., Zhou, L., An, J., Tang, L., Lu, C., Yan, W., Liu, R., Kong, S., Chen, M., Lee, S., and Yu, H.: Regional and local new particle formation events observed in the Yangtze River Delta region, China, Journal of Geophysical Research: Atmospheres, 122, 2389-2402, https://doi.org/10.1002/2016jd026030, 2017.

Dal Maso, M., Kulmala, M., Lehtinen, K. E. J., Mäkelä, J. M., Aalto, P., and O'Dowd, C. D.: Condensation and coagulation sinks and formation of nucleation mode particles in coastal and boreal forest boundary layers, Journal of Geophysical Research, 107, PAR 2-1-PAR 2-10, https://doi.org/10.1029/2001jd001053, 2002.

Dal Maso, M., Kulmala, M., Riipinen, I., Wagner, R., Hussein, T., Aalto, P. P., and Lehtinen, K. E.: Formation and growth of fresh atmospheric aerosols: eight years of aerosol size distribution data from SMEAR II, Hyytiala, Finland, Boreal environment research, 10, 323, 2005.

Dal Maso, M., Sogacheva, L., Aalto, P. P., Riipinen, I., Komppula, M., Tunved, P., Korhonen, L., Suur-Uski, V., Hirsikko, A., KurtéN, T., Kerminen, V.-M., Lihavainen, H., Viisanen, Y., Hansson, H.-C., and Kulmala, M.: Aerosol size distribution measurements at four Nordic field stations: identification, analysis and trajectory analysis of new particle formation bursts, Tellus B: Chemical and Physical Meteorology, 59, 350-361, https://doi.org/10.1111/j.1600-0889.2007.00267.x, 2007.

Dal Maso, M., Sogacheva, L., Anisimov, M. P., Arshinov, M., Baklanov, A., Belan, B., Khodzher, T. V., Obolkin, V. A., Staroverova, A., and Vlasov, A. J. B. e. r.: Aerosol particle formation events at two Siberian stations inside the boreal forest, Journal of Boreal environment research, 13, 2008.

Dall´Osto, M., Beddows, D. C. S., Tunved, P., Krejci, R., Ström, J., Hansson, H. C., Yoon, Y. J., Park, K.-T., Becagli, S., Udisti, R., Onasch, T., O´Dowd, C. D., Simó, R., and Harrison, R. M.: Arctic sea ice melt leads to atmospheric new particle formation, Scientific Reports, 7, 3318, https://doi.org/10.1038/s41598-017-03328-1, 2017.

Dall'Osto, M., Beddows, D. C. S., Asmi, A., Poulain, L., Hao, L., Freney, E., Allan, J. D., Canagaratna, M., Crippa, M., Bianchi, F., de Leeuw, G., Eriksson, A., Swietlicki, E., Hansson, H. C., Henzing, J. S., Granier, C., Zemankova, K., Laj, P., Onasch, T., Prevot, A., Putaud, J. P., Sellegri, K., Vidal, M., Virtanen, A., Simo, R., Worsnop, D., O'Dowd, C., Kulmala, M., and Harrison, R. M.: Novel insights on new particle formation derived from a pan-european observing system, Scientific Reports, 8, 1482, 10.1038/s41598-017-17343-9, 2018.

Davies, L., and Gather, U.: The Identification of Multiple Outliers, Journal of the American Statistical Association, 88, 782-792, https://doi.org/10.1080/01621459.1993.10476339, 1993.

Debevec, C., Sauvage, S., Gros, V., Sellegri, K., Sciare, J., Pikridas, M., Stavroulas, I., Leonardis, T., Gaudion, V., Depelchin, L., Fronval, I., Sarda-Esteve, R., Baisnée, D., Bonsang, B., Savvides, C., Vrekoussis, M., and Locoge, N.: Driving parameters of biogenic volatile organic compounds and consequences on new particle formation observed at an eastern Mediterranean background site, Atmospheric Chemistry and Physics, 18, 14297-14325, https://doi.org/10.5194/acp-18-14297-2018, 2018.

Drinovec, L., Sciare, J., Stavroulas, I., Bezantakos, S., Pikridas, M., Unga, F., Savvides, C., Višić, B., Remškar, M., and Močnik, G.: A new optical-based technique for real-time measurements of mineral dust concentration in PM10 using a virtual impactor, Atmospheric Measurement Techniques, 13, 3799-3813, https://doi.org/10.5194/amt-13-3799-2020, 2020.

Ehn, M., Thornton, J. A., Kleist, E., Sipilä, M., Junninen, H., Pullinen, I., Springer, M., Rubach, F., Tillmann, R., Lee, B., Lopez-Hilfiker, F., Andres, S., Acir, I.-H., Rissanen, M., Jokinen, T., Schobesberger, S., Kangasluoma, J., Kontkanen, J., Nieminen, T., Kurtén, T., Nielsen, L. B., Jørgensen, S., Kjaergaard, H. G., Canagaratna, M., Maso, M. D., Berndt, T., Petäjä, T., Wahner, A., Kerminen, V.-M., Kulmala, M., Worsnop, D. R., Wildt, J., and Mentel, T. F.: A large source of low-volatility secondary organic aerosol, Nature, 506, 476-479, https://doi.org/10.1038/nature13032, 2014.

Flanders Marine Institute: Maritime Boundaries Geodatabase: Maritime Boundaries and Exclusive Economic Zones (200NM), version 11. , Available online at http://www.marineregions.org/. https://doi.org/10.14284/386, 2019.

Fu, Y., Xue, M., Cai, R., Kangasluoma, J., and Jiang, J.: Theoretical and experimental analysis of the core sampling method: Reducing diffusional losses in aerosol sampling line, Aerosol Science and Technology, 53, 793-801, https://doi.org/10.1080/02786826.2019.1608354, 2019.

Fuchs, N. A.: The mechanics of aerosols. Translated by R. E. Daisley and Marina Fuchs; Edited by C. N. Davies., Pergamon Press, London, 1964.

Fuchs, N. A., and Sutugin, A. G.: High-dispersed aerosols, in: Topics in Current Aerosol Research, edited by: Hidy, G. M., and Brock, J. R., Pergamon, 1, 1971.

Fuller, E. N., Schettler, P. D., and Giddings, J. C.: New method for prediction of binary gas-phase diffusion coefficients, Industrial & Engineering Chemistry, 58, 18-27, https://doi.org/10.1021/ie50677a007, 1966.

Gagné, S., Lehtipalo, K., Manninen, H. E., Nieminen, T., Schobesberger, S., Franchin, A., Yli-Juuti, T., Boulon, J., Sonntag, A., Mirme, S., Mirme, A., Hõrrak, U., Petäjä, T., Asmi, E., and Kulmala, M.: Intercomparison of air ion spectrometers: an evaluation of results in varying conditions, Atmospheric Measurement Techniques, 4, 805-822, https://doi.org/10.5194/amt-4-805-2011, 2011.

Giorgi, F., and Lionello, P.: Climate change projections for the Mediterranean region, Global and Planetary Change, 63, 90-104, https://doi.org/10.1016/j.gloplacha.2007.09.005, 2008.

Gong, X., Wex, H., Müller, T., Wiedensohler, A., Höhler, K., Kandler, K., Ma, N., Dietel, B., Schiebel, T., Möhler, O., and Stratmann, F.: Characterization of aerosol properties at Cyprus, focusing on cloud condensation nuclei and ice nucleating particles, Atmospheric Chemistry and Physics Discussions, 2019, 1-34, https://doi.org/10.5194/acp-2019-198, 2019.

Gordon, H., Kirkby, J., Baltensperger, U., Bianchi, F., Breitenlechner, M., Curtius, J., Dias, A., Dommen, J., Donahue, N. M., Dunne, E. M., Duplissy, J., Ehrhart, S., Flagan, R. C., Frege, C., Fuchs, C., Hansel, A., Hoyle, C. R., Kulmala, M., Kürten, A., Lehtipalo, K., Makhmutov, V., Molteni, U., Rissanen, M. P., Stozhkov, Y., Tröstl, J., Tsagkogeorgas, G., Wagner, R., Williamson, C., Wimmer, D., Winkler, P. M., Yan, C., and Carslaw, K. S.: Causes and importance of new particle formation in the present-day and preindustrial atmospheres, 122, 8739-8760, https://doi.org/10.1002/2017jd026844, 2017.

Gormley, P. G., and Kennedy, M.: Diffusion from a Stream Flowing through a Cylindrical Tube, Proceedings of the Royal Irish Academy. Section A: Mathematical and Physical Sciences, 52, 163-169, 1948.

Greene, C. A., Thirumalai, K., Kearney, K. A., Delgado, J. M., Schwanghart, W., Wolfenbarger, N. S., Thyng, K. M., Gwyther, D. E., Gardner, A. S., and Blankenship, D. D.: The Climate Data Toolbox for MATLAB, Geochemistry, Geophysics, Geosystems, 20, 3774-3781, https://doi.org/10.1029/2019GC008392, 2019.

Größ, J., Hamed, A., Sonntag, A., Spindler, G., Manninen, H. E., Nieminen, T., Kulmala, M., Hõrrak, U., Plass-Dülmer, C., Wiedensohler, A., and Birmili, W.: Atmospheric new particle formation at the research station Melpitz, Germany: connection with gaseous precursors and meteorological parameters, Atmospheric Chemistry and Physics, 18, 1835-1861, https://doi.org/10.5194/acp-18-1835-2018, 2018.

Hakala, S., Alghamdi, M. A., Paasonen, P., Vakkari, V., Khoder, M. I., Neitola, K., Dada, L., Abdelmaksoud, A. S., Al-Jeelani, H., Shabbaj, I. I., Almehmadi, F. M., Sundström, A. M., Lihavainen, H., Kerminen, V. M., Kontkanen, J., Kulmala, M., Hussein, T., and Hyvärinen, A. P.: New particle formation, growth and apparent shrinkage at a rural background site in western Saudi Arabia, Atmospheric Chemistry and Physics, 19, 10537-10555, https://doi.org/10.5194/acp-19-10537-2019, 2019.

Hamed, A., Joutsensaari, J., Mikkonen, S., Sogacheva, L., Dal Maso, M., Kulmala, M., Cavalli, F., Fuzzi, S., Facchini, M. C., Decesari, S., Mircea, M., Lehtinen, K. E. J., and Laaksonen, A.: Nucleation and growth of new particles in Po Valley, Italy, Atmospheric Chemistry and Physics, 7, 355-376, https://doi.org/10.5194/acp-7-355-2007, 2007.

Hirsikko, A., Bergman, T., Laakso, L., Dal Maso, M., Riipinen, I., Hõrrak, U., and Kulmala, M.: Identification and classification of the formation of intermediate ions measured in boreal forest, Atmospheric Chemistry and Physics, 7, 201-210, https://doi.org/10.5194/acp-7-201-2007, 2007.

Hirsikko, A., Vakkari, V., Tiitta, P., Manninen, H. E., Gagné, S., Laakso, H., Kulmala, M., Mirme, A., Mirme, S., Mabaso, D., Beukes, J. P., and Laakso, L.: Characterisation of sub-micron particle number concentrations and formation events in the western Bushveld Igneous Complex, South Africa, Atmospheric Chemistry and Physics, 12, 3951-3967, https://doi.org/10.5194/acp-12-3951-2012, 2012.

Hirsikko, A., Vakkari, V., Tiitta, P., Hatakka, J., Kerminen, V. M., Sundström, A. M., Beukes, J. P., Manninen, H. E., Kulmala, M., and Laakso, L.: Multiple daytime nucleation events in semi-clean savannah and industrial environments in South Africa: analysis based on observations, Atmospheric Chemistry and Physics, 13, 5523-5532, https://doi.org/10.5194/acp-13-5523-2013, 2013.

Hussein, T., Martikainen, J., Junninen, H., Sogacheva, L., Wagner, R., Maso, M. D., Riipinen, I., Aalto, P. P., and Kulmala, M.: Observation of regional new particle formation in the urban atmosphere, Tellus B: Chemical and Physical Meteorology, 60, 509-521, https://doi.org/10.1111/j.1600-0889.2008.00365.x, 2008.

Hussein, T., Atashi, N., Sogacheva, L., Hakala, S., Dada, L., Petäjä, T., and Kulmala, M.: Characterization of Urban New Particle Formation in Amman—Jordan, Atmosphere, 11, 79, https://doi.org/10.3390/atmos11010079, 2020.

Jokinen, T., Kontkanen, J., Lehtipalo, K., Manninen, H. E., Aalto, J., Porcar-Castell, A., Garmash, O., Nieminen, T., Ehn, M., Kangasluoma, J., Junninen, H., Levula, J., Duplissy, J., Ahonen, L. R., Rantala, P., Heikkinen, L., Yan, C., Sipilä, M., Worsnop, D. R., Bäck, J., Petäjä, T., Kerminen, V.-M., and Kulmala, M.: Solar eclipse demonstrating the importance of photochemistry in new particle formation, Scientific Reports, 7, 45707, https://doi.org/10.1038/srep45707, 2017.

Jun, Y.-S., Jeong, C.-H., Sabaliauskas, K., Richard Leaitch, W., and Evans, G. J.: A year-long comparison of particle formation events at paired urban and rural locations, Atmospheric Pollution Research, 5, 447-454, https://doi.org/10.5094/APR.2014.052, 2014.

Kalivitis, N., Stavroulas, I., Bougiatioti, A., Kouvarakis, G., Gagné, S., Manninen, H. E., Kulmala, M., and Mihalopoulos, N.: Night-time enhanced atmospheric ion concentrations in the marine boundary layer, Atmospheric Chemistry and Physics, 12, 3627-3638, https://doi.org/10.5194/acp-12-3627-2012, 2012.

Kalivitis, N., Kerminen, V. M., Kouvarakis, G., Stavroulas, I., Bougiatioti, A., Nenes, A., Manninen, H. E., Petäjä, T., Kulmala, M., and Mihalopoulos, N.: Atmospheric new particle formation as a source of CCN in the eastern Mediterranean marine boundary layer, Atmospheric Chemistry and Physics, 15, 9203-9215, https://doi.org/10.5194/acp-15-9203-2015, 2015.

Kalivitis, N., Kerminen, V. M., Kouvarakis, G., Stavroulas, I., Tzitzikalaki, E., Kalkavouras, P., Daskalakis, N., Myriokefalitakis, S., Bougiatioti, A., Manninen, H. E., Roldin, P., Petäjä, T., Boy, M., Kulmala, M., Kanakidou, M., and Mihalopoulos, N.: Formation and growth of atmospheric nanoparticles in the eastern Mediterranean: results from long-term measurements and process simulations, Atmospheric Chemistry and Physics, 19, 2671-2686, https://doi.org/10.5194/acp-19-2671-2019, 2019.

Kalkavouras, P., Bossioli, E., Bezantakos, S., Bougiatioti, A., Kalivitis, N., Stavroulas, I., Kouvarakis, G., Protonotariou, A. P., Dandou, A., Biskos, G., Mihalopoulos, N., Nenes, A., and Tombrou, M.: New particle formation in the southern Aegean Sea during the Etesians: importance for CCN production and cloud droplet number, Atmospheric Chemistry and Physics, 17, 175-192, https://doi.org/10.5194/acp-17-175-2017, 2017.

Kalkavouras, P., Bougiatioti, A., Kalivitis, N., Stavroulas, I., Tombrou, M., Nenes, A., and Mihalopoulos, N.: Regional new particle formation as modulators of cloud condensation nuclei and cloud droplet number in

the eastern Mediterranean, Atmospheric chemistry and Physics, 19, 6185-6203,
https://doi.org/10.5194/acp-19-6185-2019, 2019.

Kalkavouras, P., Bougiatioti, A., Grivas, G., Stavroulas, I., Kalivitis, N., Liakakou, E., Gerasopoulos, E., Pilinis, C., and Mihalopoulos, N.: On the regional aspects of new particle formation in the Eastern Mediterranean: A comparative study between a background and an urban site based on long term observations, Atmospheric Research, 239, 104911, https://doi.org/10.1016/j.atmosres.2020.104911, 2020.

Kammer, J., Perraudin, E., Flaud, P. M., Lamaud, E., Bonnefond, J. M., and Villenave, E.: Observation of nighttime new particle formation over the French Landes forest, Science of The Total Environment, 621, 1084-1092, https://doi.org/10.1016/j.scitotenv.2017.10.118, 2018.

Kangasluoma, J., Cai, R., Jiang, J., Deng, C., Stolzenburg, D., Ahonen, L. R., Chan, T., Fu, Y., Kim, C., Laurila, T. M., Zhou, Y., Dada, L., Sulo, J., Flagan, R. C., Kulmala, M., Petäjä, T., and Lehtipalo, K.: Overview of measurements and current instrumentation for 1–10 nm aerosol particle number size distributions, Journal of Aerosol Science, 105584, https://doi.org/10.1016/j.jaerosci.2020.105584, 2020.

Kerminen, V.-M., Chen, X., Vakkari, V., Petäjä, T., Kulmala, M., and Bianchi, F.: Atmospheric new particle formation and growth: review of field observations, Environmental Research Letters, 13, 103003, https://doi.org/10.1088/1748-9326/aadf3c, 2018.

Kerminen, V. M., Paramonov, M., Anttila, T., Riipinen, I., Fountoukis, C., Korhonen, H., Asmi, E., Laakso, L., Lihavainen, H., Swietlicki, E., Svenningsson, B., Asmi, A., Pandis, S. N., Kulmala, M., and Petäjä, T.: Cloud condensation nuclei production associated with atmospheric nucleation: a synthesis based on existing literature and new results, Atmospheric Chemistry and Physics, 12, 12037-12059, https://doi.org/10.5194/acp-12-12037-2012, 2012.

Kirkby, J., Curtius, J., Almeida, J., Dunne, E., Duplissy, J., Ehrhart, S., Franchin, A., Gagné, S., Ickes, L., Kürten, A., Kupc, A., Metzger, A., Riccobono, F., Rondo, L., Schobesberger, S., Tsagkogeorgas, G., Wimmer, D., Amorim, A., Bianchi, F., Breitenlechner, M., David, A., Dommen, J., Downard, A., Ehn, M., Flagan, R. C., Haider, S., Hansel, A., Hauser, D., Jud, W., Junninen, H., Kreissl, F., Kvashin, A., Laaksonen, A., Lehtipalo, K., Lima, J., Lovejoy, E. R., Makhmutov, V., Mathot, S., Mikkilä, J., Minginette, P., Mogo, S., Nieminen, T., Onnela, A., Pereira, P., Petäjä, T., Schnitzhofer, R., Seinfeld, J. H., Sipilä, M., Stozhkov, Y., Stratmann, F., Tomé, A., Vanhanen, J., Viisanen, Y., Vrtala, A., Wagner, P. E., Walther, H., Weingartner, E., Wex, H., Winkler, P. M., Carslaw, K. S., Worsnop, D. R., Baltensperger, U., and Kulmala, M.: Role of sulphuric acid, ammonia and galactic cosmic rays in atmospheric aerosol nucleation, Nature, 476, 429-433, https://doi.org/10.1038/nature10343, 2011.

Kivekäs, N., Carpman, J., Roldin, P., Leppä, J., O'Connor, E., Kristensson, A., and Asmi, E.: Coupling an aerosol box model with one-dimensional flow: a tool for understanding observations of new particle formation events, Tellus B: Chemical and Physical Meteorology, 68, 29706, https://doi.org/10.3402/tellusb.v68.29706, 2016.

Kleanthous, S., Vrekoussis, M., Mihalopoulos, N., Kalabokas, P., and Lelieveld, J.: On the temporal and spatial variation of ozone in Cyprus, Science of The Total Environment, 476-477, 677-687, https://doi.org/10.1016/j.scitotenv.2013.12.101, 2014.

Kopanakis, I., Chatoutsidou, S. E., Torseth, K., Glytsos, T., and Lazaridis, M.: Particle number size distribution in the eastern Mediterranean: Formation and growth rates of ultrafine airborne atmospheric particles, Atmospheric Environment, 77, 790-802, https://doi.org/10.1016/j.atmosenv.2013.05.066, 2013.

Kostopoulou, E., and Jones, P. D.: Comprehensive analysis of the climate variability in the eastern Mediterranean. Part I: map-pattern classification, International Journal of Climatology, 27, 1189-1214, https://doi.org/10.1002/joc.1467, 2007a.

Kostopoulou, E., and Jones, P. D.: Comprehensive analysis of the climate variability in the eastern Mediterranean. Part II: relationships between atmospheric circulation patterns and surface climatic elements, International Journal of Climatology, 27, 1351-1371, https://doi.org/10.1002/joc.1466, 2007b.

Kristensson, A., Dal Maso, M., Swietlicki, E., Hussein, T., Zhou, J., Kerminen, V. M., and Kulmala, M.: Characterization of new particle formation events at a background site in Southern Sweden: relation to air mass history, Tellus B: Chemical and Physical Meteorology, 60, 330-344, https://doi.org/10.1111/j.1600-0889.2008.00345.x, 2008.

Kulmala, M., Maso, M. D., Mäkelä, J. M., Pirjola, L., Väkevä, M., Aalto, P., Miikkulainen, P., Hämeri, K., and O'dowd, C. D.: On the formation, growth and composition of nucleation mode particles, Tellus B: Chemical and Physical Meteorology, 53, 479-490, https://doi.org/10.3402/tellusb.v53i4.16622, 2001.

Kulmala, M., Petäjä, T., Nieminen, T., Sipilä, M., Manninen, H. E., Lehtipalo, K., Dal Maso, M., Aalto, P. P., Junninen, H., Paasonen, P., Riipinen, I., Lehtinen, K. E. J., Laaksonen, A., and Kerminen, V.-M.: Measurement of the nucleation of atmospheric aerosol particles, Nature Protocols, 7, 1651-1667, https://doi.org/10.1038/nprot.2012.091, 2012.

Kulmala, M., Kontkanen, J., Junninen, H., Lehtipalo, K., Manninen, H. E., Nieminen, T., Petäjä, T., Sipilä, M., Schobesberger, S., Rantala, P., Franchin, A., Jokinen, T., Järvinen, E., Äijälä, M., Kangasluoma, J., Hakala, J., Aalto, P. P., Paasonen, P., Mikkilä, J., Vanhanen, J., Aalto, J., Hakola, H., Makkonen, U., Ruuskanen, T., Mauldin, R. L., Duplissy, J., Vehkamäki, H., Bäck, J., Kortelainen, A., Riipinen, I., Kurtén, T., Johnston, M. V., Smith, J. N., Ehn, M., Mentel, T. F., Lehtinen, K. E. J., Laaksonen, A., Kerminen, V.-M., and Worsnop, D. R.: Direct Observations of Atmospheric Aerosol Nucleation, Science, 339, 943-946, https://doi.org/10.1126/science.1227385 2013.

Kulmala, M., Petäjä, T., Ehn, M., Thornton, J., Sipilä, M., Worsnop, D. R., and Kerminen, V.-M.: Chemistry of Atmospheric Nucleation: On the Recent Advances on Precursor Characterization and Atmospheric Cluster Composition in Connection with Atmospheric New Particle Formation, Annual Review of Physical Chemistry, 65, 21-37, https://doi.org/10.1146/annurev-physchem-040412-110014, 2014.

Kulmala, M., Kerminen, V. M., Petäjä, T., Ding, A. J., and Wang, L.: Atmospheric gas-to-particle conversion: why NPF events are observed in megacities?, Faraday Discussions, 200, 271-288, https://doi.org/10.1039/C6FD00257A, 2017.

Kürten, A., Li, C., Bianchi, F., Curtius, J., Dias, A., Donahue, N. M., Duplissy, J., Flagan, R. C., Hakala, J., Jokinen, T., Kirkby, J., Kulmala, M., Laaksonen, A., Lehtipalo, K., Makhmutov, V., Onnela, A., Rissanen, M. P., Simon, M., Sipilä, M., Stozhkov, Y., Tröstl, J., Ye, P., and McMurry, P. H.: New particle formation in the sulfuric acid–dimethylamine–water system: reevaluation of CLOUD chamber measurements and comparison to an aerosol nucleation and growth model, Atmospheric Chemistry and Physics, 18, 845-863, https://doi.org/10.5194/acp-18-845-2018, 2018.

Kurten, T., Loukonen, V., Vehkamaki, H., and Kulmala, M.: Amines are likely to enhance neutral and ion-induced sulfuric acid-water nucleation in the atmosphere more effectively than ammonia, Atmospheric Chemistry and Physics, 8, 4095-4103, https://doi.org/10.5194/acp-8-4095-2008, 2008.

Laaksonen, A., Hamed, A., Joutsensaari, J., Hiltunen, L., Cavalli, F., Junkermann, W., Asmi, A., Fuzzi, S., and Facchini, M. C.: Cloud condensation nucleus production from nucleation events at a highly polluted region, Geophysical Research Letters, 32, https://doi.org/10.1029/2004GL022092, 2005.

Lee, H., Lee, K., Lunder, C. R., Krejci, R., Aas, W., Park, J., Park, K. T., Lee, B. Y., Yoon, Y. J., and Park, K.: Atmospheric new particle formation characteristics in the Arctic as measured at Mount Zeppelin, Svalbard, from 2016 to 2018, Atmospheric Chemistry and Physics Discussions, 2020, 1-28, https://doi.org/10.5194/acp-2020-390, 2020.

Atmospheric
Chemistry
and Physics
Discussions

Lee, S.-H., Gordon, H., Yu, H., Lehtipalo, K., Haley, R., Li, Y., and Zhang, R.: New Particle Formation in the Atmosphere: From Molecular Clusters to Global Climate, Journal of Geophysical Research: Atmospheres, 124, 7098-7146, https://doi.org/10.1029/2018jd029356, 2019.

Lehtipalo, K., Sipilä, M., Junninen, H., Ehn, M., Berndt, T., Kajos, M. K., Worsnop, D. R., Petäjä, T., and Kulmala, M.: Observations of Nano-CN in the Nocturnal Boreal Forest, Aerosol Science and Technology, 45, 499-509, https://doi.org/10.1080/02786826.2010.547537, 2011.

Lehtipalo, K., Leppä, J., Kontkanen, J., Kangasluoma, J., Franchin, A., Wimmer, D., Schobesberger, S., Junninen, H., Petäjä, T., and Sipilä, M.: Methods for determining particle size distribution and growth rates between 1 and 3 nm using the Particle Size Magnifier, Boreal Environment Research, 19, 215–236, 2014.

Lehtipalo, K., Rondo, L., Kontkanen, J., Schobesberger, S., Jokinen, T., Sarnela, N., Kürten, A., Ehrhart, S., Franchin, A., Nieminen, T., Riccobono, F., Sipilä, M., Yli-Juuti, T., Duplissy, J., Adamov, A., Ahlm, L., Almeida, J., Amorim, A., Bianchi, F., Breitenlechner, M., Dommen, J., Downard, A. J., Dunne, E. M., Flagan, R. C., Guida, R., Hakala, J., Hansel, A., Jud, W., Kangasluoma, J., Kerminen, V.-M., Keskinen, H., Kim, J., Kirkby, J., Kupc, A., Kupiainen-Määttä, O., Laaksonen, A., Lawler, M. J., Leiminger, M., Mathot, S., Olenius, T., Ortega, I. K., Onnela, A., Petäjä, T., Praplan, A., Rissanen, M. P., Ruuskanen, T., Santos, F. D., Schallhart, S., Schnitzhofer, R., Simon, M., Smith, J. N., Tröstl, J., Tsagkogeorgas, G., Tomé, A., Vaattovaara, P., Vehkamäki, H., Vrtala, A. E., Wagner, P. E., Williamson, C., Wimmer, D., Winkler, P. M., Virtanen, A., Donahue, N. M., Carslaw, K. S., Baltensperger, U., Riipinen, I., Curtius, J., Worsnop, D. R., and Kulmala, M.: The effect of acid–base clustering and ions on the growth of atmospheric nano-particles, Nature Communications, 7, 11594, https://doi.org/10.1038/ncomms11594, 2016.

Leino, K., Nieminen, T., Manninen, H. E., Petäjä, T., Kerminen, V.-M., and Kulmala, M.: Intermediate ions as a strong indicator of new particle formation bursts in a boreal forest, Boreal Environment Research, 21, 274-286, 2016.

Lelieveld, J., Berresheim, H., Borrmann, S., Crutzen, P. J., Dentener, F. J., Fischer, H., Feichter, J., Flatau, P. J., Heland, J., Holzinger, R., Korrmann, R., Lawrence, M. G., Levin, Z., Markowicz, K. M., Mihalopoulos, N., Minikin, A., Ramanathan, V., de Reus, M., Roelofs, G. J., Scheeren, H. A., Sciare, J., Schlager, H., Schultz, M., Siegmund, P., Steil, B., Stephanou, E. G., Stier, P., Traub, M., Warneke, C., Williams, J., and Ziereis, H.: Global Air Pollution Crossroads over the Mediterranean, Science, 298, 794-799, https://doi.org/10.1126/science.1075457, 2002.

Lelieveld, J., Proestos, Y., Hadjinicolaou, P., Tanarhte, M., Tyrlis, E., and Zittis, G.: Strongly increasing heat extremes in the Middle East and North Africa (MENA) in the 21st century, Climatic Change, 137, 245-260, https://doi.org/10.1007/s10584-016-1665-6, 2016.

Lu, Y., Yan, C., Fu, Y., Chen, Y., Liu, Y., Yang, G., Wang, Y., Bianchi, F., Chu, B., Zhou, Y., Yin, R., Baalbaki, R., Garmash, O., Deng, C., Wang, W., Liu, Y., Petäjä, T., Kerminen, V. M., Jiang, J., Kulmala, M., and Wang, L.: A proxy for atmospheric daytime gaseous sulfuric acid concentration in urban Beijing, Atmospheric Chemistry and Physics, 19, 1971-1983, https://doi.org/10.5194/acp-19-1971-2019, 2019.

Manninen, H. E., Nieminen, T., Asmi, E., Gagné, S., Häkkinen, S., Lehtipalo, K., Aalto, P., Vana, M., Mirme, A., Mirme, S., Hõrrak, U., Plass-Dülmer, C., Stange, G., Kiss, G., Hoffer, A., Törő, N., Moerman, M., Henzing, B., de Leeuw, G., Brinkenberg, M., Kouvarakis, G. N., Bougiatioti, A., Mihalopoulos, N., O'Dowd, C., Ceburnis, D., Arneth, A., Svenningsson, B., Swietlicki, E., Tarozzi, L., Decesari, S., Facchini, M. C., Birmili, W., Sonntag, A., Wiedensohler, A., Boulon, J., Sellegri, K., Laj, P., Gysel, M., Bukowiecki, N., Weingartner, E., Wehrle, G., Laaksonen, A., Hamed, A., Joutsensaari, J., Petäjä, T., Kerminen, V. M., and Kulmala, M.: EUCAARI ion spectrometer measurements at 12 European sites – analysis of new particle formation events, Atmospheric Chemistry and Physics, 10, 7907-7927, https://doi.org/10.5194/acp-10-7907-2010, 2010.

Manninen, H. E., Mirme, S., Mirme, A., Petäjä, T., and Kulmala, M.: How to reliably detect molecular clusters and nucleation mode particles with Neutral cluster and Air Ion Spectrometer (NAIS), Journal of Atmospheric Measurement Techniques, 9, 3577-3605, https://doi.org/10.5194/amt-9-3577-2016, 2016.

Merikanto, J., Spracklen, D. V., Mann, G. W., Pickering, S. J., and Carslaw, K. S.: Impact of nucleation on global CCN, Atmospheric Chemistry and Physics, 9, 8601-8616, https://doi.org/10.5194/acp-9-8601-2009, 2009.

Mikkonen, S., Romakkaniemi, S., Smith, J. N., Korhonen, H., Petäjä, T., Plass-Duelmer, C., Boy, M., McMurry, P. H., Lehtinen, K. E. J., Joutsensaari, J., Hamed, A., Mauldin Iii, R. L., Birmili, W., Spindler, G., Arnold, F., Kulmala, M., and Laaksonen, A.: A statistical proxy for sulphuric acid concentration, Atmospheric Chemistry and Physics, 11, 11319-11334, https://doi.org/10.5194/acp-11-11319-2011, 2011.

Mirme, S., and Mirme, A.: The mathematical principles and design of the NAIS–a spectrometer for the measurement of cluster ion and nanometer aerosol size distributions, Atmospheric Measurement Techniques, 6, 1061-1071, https://doi.org/10.5194/amt-6-1061-2013, 2013.

Nie, W., Ding, A., Wang, T., Kerminen, V.-M., George, C., Xue, L., Wang, W., Zhang, Q., Petäjä, T., Qi, X., Gao, X., Wang, X., Yang, X., Fu, C., and Kulmala, M.: Polluted dust promotes new particle formation and growth, Scientific Reports, 4, 6634, 10.1038/srep06634, 2014.

Nieminen, T., Kerminen, V. M., Petäjä, T., Aalto, P. P., Arshinov, M., Asmi, E., Baltensperger, U., Beddows, D. C. S., Beukes, J. P., Collins, D., Ding, A., Harrison, R. M., Henzing, B., Hooda, R., Hu, M., Hõrrak, U., Kivekäs, N., Komsaare, K., Krejci, R., Kristensson, A., Laakso, L., Laaksonen, A., Leaitch, W. R., Lihavainen, H., Mihalopoulos, N., Németh, Z., Nie, W., O'Dowd, C., Salma, I., Sellegri, K., Svenningsson, B., Swietlicki, E., Tunved, P., Ulevicius, V., Vakkari, V., Vana, M., Wiedensohler, A., Wu, Z., Virtanen, A., and Kulmala, M.: Global analysis of continental boundary layer new particle formation based on long-term measurements, Atmospheric Chemistry and Physics, 18, 14737-14756, https://doi.org/10.5194/acp-18-14737-2018, 2018.

Olenius, T., and Riipinen, I.: Molecular-resolution simulations of new particle formation: Evaluation of common assumptions made in describing nucleation in aerosol dynamics models, Aerosol Science and Technology, 51, 397-408, https://doi.org/10.1080/02786826.2016.1262530, 2017.

Pearson, R. K., Neuvo, Y., Astola, J., and Gabbouj, M.: Generalized Hampel Filters, EURASIP Journal on Advances in Signal Processing, 2016, 87, https://doi.org/10.1186/s13634-016-0383-6, 2016.

Petäjä, T., Kerminen, V. M., Dal Maso, M., Junninen, H., Koponen, I. K., Hussein, T., Aalto, P. P., Andronopoulos, S., Robin, D., Hämeri, K., Bartzis, J. G., and Kulmala, M.: Sub-micron atmospheric aerosols in the surroundings of Marseille and Athens: physical characterization and new particle formation, Atmospheric Chemistry and Physics, 7, 2705-2720, https://doi.org/10.5194/acp-7-2705-2007, 2007.

Petäjä, T., Mauldin, I. R. L., Kosciuch, E., McGrath, J., Nieminen, T., Paasonen, P., Boy, M., Adamov, A., Kotiaho, T., and Kulmala, M.: Sulfuric acid and OH concentrations in a boreal forest site, Atmospheric Chemistry and Physics, 9, 7435-7448, https://doi.org/10.5194/acp-9-7435-2009, 2009.

Petters, M. D., and Kreidenweis, S. M.: A single parameter representation of hygroscopic growth and cloud condensation nucleus activity, Atmospheric Chemistry and Physics, 7, 1961-1971, https://doi.org/10.5194/acp-7-1961-2007, 2007.

Pierce, J. R., and Adams, P. J.: Uncertainty in global CCN concentrations from uncertain aerosol nucleation and primary emission rates, Atmospheric Chemistry and Physics, 9, 1339-1356, https://doi.org/10.5194/acp-9-1339-2009, 2009.

Pikridas, M., Bougiatioti, A., Hildebrandt, L., Engelhart, G. J., Kostenidou, E., Mohr, C., Prévôt, A. S. H., Kouvarakis, G., Zarmpas, P., Burkhart, J. F., Lee, B. H., Psichoudaki, M., Mihalopoulos, N., Pilinis, C., Stohl, A., Baltensperger, U., Kulmala, M., and Pandis, S. N.: The Finokalia Aerosol Measurement Experiment – 2008

(FAME-08): an overview, Atmospheric Chemistry and Physics, 10, 6793-6806, https://doi.org/10.5194/acp-10-6793-2010, 2010.

Pikridas, M., Riipinen, I., Hildebrandt, L., Kostenidou, E., Manninen, H., Mihalopoulos, N., Kalivitis, N., Burkhart, J. F., Stohl, A., Kulmala, M., and Pandis, S. N.: New particle formation at a remote site in the eastern Mediterranean, Journal of Geophysical Research: Atmospheres, 117, https://doi.org/10.1029/2012JD017570, 2012.

Pikridas, M., Vrekoussis, M., Sciare, J., Kleanthous, S., Vasiliadou, E., Kizas, C., Savvides, C., and Mihalopoulos, N.: Spatial and temporal (short and long-term) variability of submicron, fine and sub-10 µm particulate matter (PM1, PM2.5, PM10) in Cyprus, Atmospheric Environment, 191, 79-93, https://doi.org/10.1016/j.atmosenv.2018.07.048, 2018.

Qian, S., Sakurai, H., and McMurry, P. H.: Characteristics of regional nucleation events in urban East St. Louis, Atmospheric Environment, 41, 4119-4127, https://doi.org/10.1016/j.atmosenv.2007.01.011, 2007.

Riipinen, I., Pierce, J. R., Yli-Juuti, T., Nieminen, T., Hakkinen, S., Ehn, M., Junninen, H., Lehtipalo, K., Petaja, T., Slowik, J., Chang, R., Shantz, N. C., Abbatt, J., Leaitch, W. R., Kerminen, V. M., Worsnop, D. R., Pandis, S. N., Donahue, N. M., and Kulmala, M.: Organic condensation: a vital link connecting aerosol formation to cloud condensation nuclei (CCN) concentrations, Atmospheric Chemistry and Physics, 11, 3865-3878, https://doi.org/10.5194/acp-11-3865-2011, 2011.

Rose, C., Sellegri, K., Freney, E., Dupuy, R., Colomb, A., Pichon, J. M., Ribeiro, M., Bourianne, T., Burnet, F., and Schwarzenboeck, A.: Airborne measurements of new particle formation in the free troposphere above the Mediterranean Sea during the HYMEX campaign, Atmospheric Chemistry and Physics, 15, 10203-10218, https://doi.org/10.5194/acp-15-10203-2015, 2015.

Rose, C., Zha, Q., Dada, L., Yan, C., Lehtipalo, K., Junninen, H., Mazon, S. B., Jokinen, T., Sarnela, N., Sipilä, M., Petäjä, T., Kerminen, V.-M., Bianchi, F., and Kulmala, M.: Observations of biogenic ion-induced cluster formation in the atmosphere, Science Advances, 4, eaar5218, https://doi.org/10.1126/sciadv.aar5218, 2018.

Salma, I., Borsós, T., Weidinger, T., Aalto, P., Hussein, T., Dal Maso, M., and Kulmala, M.: Production, growth and properties of ultrafine atmospheric aerosol particles in an urban environment, Atmospheric Chemistry and Physics, 11, 1339-1353, https://doi.org/10.5194/acp-11-1339-2011, 2011.

Salma, I., Németh, Z., Kerminen, V. M., Aalto, P., Nieminen, T., Weidinger, T., Molnár, Á., Imre, K., and Kulmala, M.: Regional effect on urban atmospheric nucleation, Atmospheric Chemistry and Physics, 16, 8715-8728, https://doi.org/10.5194/acp-16-8715-2016, 2016a.

Salma, I., Németh, Z., Weidinger, T., Kovács, B., and Kristóf, G.: Measurement, growth types and shrinkage of newly formed aerosol particles at an urban research platform, Atmospheric Chemistry and Physics, 16, 7837-7851, https://doi.org/10.5194/acp-16-7837-2016, 2016b.

Salma, I., and Németh, Z.: Dynamic and timing properties of new aerosol particle formation and consecutive growth events, Atmospheric Chemistry and Physics, 19, 5835-5852, https://doi.org/10.5194/acp-19-5835-2019, 2019.

Sciare, J.: The Agia Marina Xyliatou Observatory: A remote supersite in Cyprus to monitor changes in the atmospheric composition of the Eastern Mediterranean and the Middle East, EGU General Assembly Conference Abstracts, 2016,

Seinfeld, J. H., and Pandis, S. N.: Atmospheric chemistry and physics: from air pollution to climate change, John Wiley & Sons, 2012.

Siakavaras, D., Samara, C., Petrakakis, M., and Biskos, G.: Nucleation events at a coastal city during the warm period: Kerbside versus urban background measurements, Atmospheric Environment, 140, 60-68, https://doi.org/10.1016/j.atmosenv.2016.05.054, 2016.

Simon, M., Dada, L., Heinritzi, M., Scholz, W., Stolzenburg, D., Fischer, L., Wagner, A. C., Kürten, A., Rörup, B., He, X. C., Almeida, J., Baalbaki, R., Baccarini, A., Bauer, P. S., Beck, L., Bergen, A., Bianchi, F., Bräkling, S., Brilke, S., Caudillo, L., Chen, D., Chu, B., Dias, A., Draper, D. C., Duplissy, J., El-Haddad, I., Finkenzeller, H., Frege, C., Gonzalez-Carracedo, L., Gordon, H., Granzin, M., Hakala, J., Hofbauer, V., Hoyle, C. R., Kim, C., Kong, W., Lamkaddam, H., Lee, C. P., Lehtipalo, K., Leiminger, M., Mai, H., Manninen, H. E., Marie, G., Marten, R., Mentler, B., Molteni, U., Nichman, L., Nie, W., Ojdanic, A., Onnela, A., Partoll, E., Petäjä, T., Pfeifer, J., Philippov, M., Quéléver, L. L. J., Ranjithkumar, A., Rissanen, M. P., Schallhart, S., Schobesberger, S., Schuchmann, S., Shen, J., Sipilä, M., Steiner, G., Stozhkov, Y., Tauber, C., Tham, Y. J., Tomé, A. R., Vazquez-Pufleau, M., Vogel, A. L., Wagner, R., Wang, M., Wang, D. S., Wang, Y., Weber, S. K., Wu, Y., Xiao, M., Yan, C., Ye, P., Ye, Q., Zauner-Wieczorek, M., Zhou, X., Baltensperger, U., Dommen, J., Flagan, R. C., Hansel, A., Kulmala, M., Volkamer, R., Winkler, P. M., Worsnop, D. R., Donahue, N. M., Kirkby, J., and Curtius, J.: Molecular understanding of new-particle formation from α-pinene between −50 and +25 °C, Atmospheric Chemistry and Physics, 20, 9183-9207, https://doi.org/10.5194/acp-20-9183-2020, 2020.

Sipilä, M., Berndt, T., Petäjä, T., Brus, D., Vanhanen, J., Stratmann, F., Patokoski, J., Mauldin, R. L., Hyvärinen, A.-P., Lihavainen, H., and Kulmala, M.: The Role of Sulfuric Acid in Atmospheric Nucleation, Science, 327, 1243-1246, https://doi.org/10.1126/science.1180315 %J Science, 2010.

Skrabalova, L., Zikova, N., and Zdimal, V.: Shrinkage of Newly Formed Particles in an Urban Environment, Aerosol and Air Quality Research, 15, 1313-1324, https://doi.org/10.4209/aaqr.2015.01.0015, 2015.

Solomou, E., Poupkou, A., Bolis, S., Zanis, P., Lazaridis, M., and Melas, D.: Evaluating near-surface ozone levels simulated from MACC global and regional modelling systems in Eastern Mediterranean under the influence of Etesian winds, Atmospheric Research, 208, 191-200, https://doi.org/10.1016/j.atmosres.2017.09.010, 2018.

Spracklen, D. V., Carslaw, K. S., Kulmala, M., Kerminen, V. M., Mann, G. W., and Sihto, S. L.: The contribution of boundary layer nucleation events to total particle concentrations on regional and global scales, Atmospheric Chemistry and Physics, 6, 5631-5648, https://doi.org/10.5194/acp-6-5631-2006, 2006.

Spracklen, D. V., Carslaw, K. S., Kulmala, M., Kerminen, V.-M., Sihto, S.-L., Riipinen, I., Merikanto, J., Mann, G. W., Chipperfield, M. P., Wiedensohler, A., Birmili, W., and Lihavainen, H.: Contribution of particle formation to global cloud condensation nuclei concentrations, Geophysical Research Letters, 35, https://doi.org/10.1029/2007gl033038, 2008.

Stohl, A., Forster, C., Frank, A., Seibert, P., and Wotawa, G.: Technical note: The Lagrangian particle dispersion model FLEXPART version 6.2, Atmospheric Chemistry and Physics, 5, 2461-2474, https://doi.org/10.5194/acp-5-2461-2005, 2005.

Stolzenburg, D., Fischer, L., Vogel, A. L., Heinritzi, M., Schervish, M., Simon, M., Wagner, A. C., Dada, L., Ahonen, L. R., Amorim, A., Baccarini, A., Bauer, P. S., Baumgartner, B., Bergen, A., Bianchi, F., Breitenlechner, M., Brilke, S., Buenrostro Mazon, S., Chen, D., Dias, A., Draper, D. C., Duplissy, J., El Haddad, I., Finkenzeller, H., Frege, C., Fuchs, C., Garmash, O., Gordon, H., He, X., Helm, J., Hofbauer, V., Hoyle, C. R., Kim, C., Kirkby, J., Kontkanen, J., Kürten, A., Lampilahti, J., Lawler, M., Lehtipalo, K., Leiminger, M., Mai, H., Mathot, S., Mentler, B., Molteni, U., Nie, W., Nieminen, T., Nowak, J. B., Ojdanic, A., Onnela, A., Passananti, M., Petäjä, T., Quéléver, L. L. J., Rissanen, M. P., Sarnela, N., Schallhart, S., Tauber, C., Tomé, A., Wagner, R., Wang, M., Weitz, L., Wimmer, D., Xiao, M., Yan, C., Ye, P., Zha, Q., Baltensperger, U., Curtius, J., Dommen, J., Flagan, R. C., Kulmala, M., Smith, J. N., Worsnop, D. R., Hansel, A., Donahue, N. M., and Winkler, P. M.: Rapid growth of organic aerosol nanoparticles over a wide tropospheric temperature range, Proceedings of the National Academy of Sciences, 115, 9122, https://doi.org/10.1073/pnas.1807604115, 2018.

Tröstl, J., Chuang, W. K., Gordon, H., Heinritzi, M., Yan, C., Molteni, U., Ahlm, L., Frege, C., Bianchi, F., Wagner, R., Simon, M., Lehtipalo, K., Williamson, C., Craven, J. S., Duplissy, J., Adamov, A., Almeida, J., Bernhammer, A.-K., Breitenlechner, M., Brilke, S., Dias, A., Ehrhart, S., Flagan, R. C., Franchin, A., Fuchs, C., Guida, R., Gysel, M., Hansel, A., Hoyle, C. R., Jokinen, T., Junninen, H., Kangasluoma, J., Keskinen, H., Kim, J., Krapf, M., Kürten, A., Laaksonen, A., Lawler, M., Leiminger, M., Mathot, S., Möhler, O., Nieminen, T., Onnela, A., Petäjä, T., Piel, F. M., Miettinen, P., Rissanen, M. P., Rondo, L., Sarnela, N., Schobesberger, S., Sengupta, K., Sipilä, M., Smith, J. N., Steiner, G., Tomè, A., Virtanen, A., Wagner, A. C., Weingartner, E., Wimmer, D., Winkler, P. M., Ye, P., Carslaw, K. S., Curtius, J., Dommen, J., Kirkby, J., Kulmala, M., Riipinen, I., Worsnop, D. R., Donahue, N. M., and Baltensperger, U.: The role of low-volatility organic compounds in initial particle growth in the atmosphere, Nature, 533, 527-531, https://doi.org/10.1038/nature18271, 2016.

Tsagkogeorgas, G., Roldin, P., Duplissy, J., Rondo, L., Tröstl, J., Slowik, J. G., Ehrhart, S., Franchin, A., Kürten, A., Amorim, A., Bianchi, F., Kirkby, J., Petäjä, T., Baltensperger, U., Boy, M., Curtius, J., Flagan, R. C., Kulmala, M., Donahue, N. M., and Stratmann, F.: Evaporation of sulfate aerosols at low relative humidity, Atmospheric Chemistry and Physics, 17, 8923-8938, https://doi.org/10.5194/acp-17-8923-2017, 2017.

Tyrlis, E., and Lelieveld, J.: Climatology and Dynamics of the Summer Etesian Winds over the Eastern Mediterranean, Journal of the Atmospheric Sciences, 70, 3374-3396, https://doi.org/10.1175/JAS-D-13-035.1, 2013.

Ulbrich, U., Lionello, P., Belušić, D., Jacobeit, J., Knippertz, P., Kuglitsch, F. G., Leckebusch, G. C., Luterbacher, J., Maugeri, M., Maheras, P., Nissen, K. M., Pavan, V., Pinto, J. G., Saaroni, H., Seubert, S., Toreti, A., Xoplaki, E., and Ziv, B.: 5 - Climate of the Mediterranean: Synoptic Patterns, Temperature, Precipitation, Winds, and Their Extremes, in: The Climate of the Mediterranean Region, edited by: Lionello, P., Elsevier, Oxford, 301-346, 2012.

Vakkari, V., Laakso, H., Kulmala, M., Laaksonen, A., Mabaso, D., Molefe, M., Kgabi, N., and Laakso, L.: New particle formation events in semi-clean South African savannah, Atmospheric Chemistry and Physics, 11, 3333-3346, https://doi.org/10.5194/acp-11-3333-2011, 2011.

Vanhanen, J., Mikkilä, J., Lehtipalo, K., Sipilä, M., Manninen, H. E., Siivola, E., Petäjä, T., and Kulmala, M.: Particle Size Magnifier for Nano-CN Detection, Aerosol Science and Technology, 45, 533-542, https://doi.org/10.1080/02786826.2010.547889, 2011.

Wang, M., and Penner, J. E.: Aerosol indirect forcing in a global model with particle nucleation, Atmospheric Chemistry and Physics, 9, 239-260, https://doi.org/10.5194/acp-9-239-2009, 2009.

Wang, M., Kong, W., Marten, R., He, X.-C., Chen, D., Pfeifer, J., Heitto, A., Kontkanen, J., Dada, L., Kürten, A., Yli-Juuti, T., Manninen, H. E., Amanatidis, S., Amorim, A., Baalbaki, R., Baccarini, A., Bell, D. M., Bertozzi, B., Bräkling, S., Brilke, S., Murillo, L. C., Chiu, R., Chu, B., De Menezes, L.-P., Duplissy, J., Finkenzeller, H., Carracedo, L. G., Granzin, M., Guida, R., Hansel, A., Hofbauer, V., Krechmer, J., Lehtipalo, K., Lamkaddam, H., Lampimäki, M., Lee, C. P., Makhmutov, V., Marie, G., Mathot, S., Mauldin, R. L., Mentler, B., Müller, T., Onnela, A., Partoll, E., Petäjä, T., Philippov, M., Pospisilova, V., Ranjithkumar, A., Rissanen, M., Rörup, B., Scholz, W., Shen, J., Simon, M., Sipilä, M., Steiner, G., Stolzenburg, D., Tham, Y. J., Tomé, A., Wagner, A. C., Wang, D. S., Wang, Y., Weber, S. K., Winkler, P. M., Wlasits, P. J., Wu, Y., Xiao, M., Ye, Q., Zauner-Wieczorek, M., Zhou, X., Volkamer, R., Riipinen, I., Dommen, J., Curtius, J., Baltensperger, U., Kulmala, M., Worsnop, D. R., Kirkby, J., Seinfeld, J. H., El-Haddad, I., Flagan, R. C., and Donahue, N. M.: Rapid growth of new atmospheric particles by nitric acid and ammonia condensation, Nature, 581, 184-189, https://doi.org/10.1038/s41586-020-2270-4, 2020.

Wang, S. C., and Flagan, R. C.: Scanning Electrical Mobility Spectrometer, Aerosol Science and Technology, 13, 230-240, https://doi.org/10.1080/02786829008959441, 1990.

Weber, R. J., Marti, J. J., McMurry, P. H., Eisele, F. L., Tanner, D. J., and Jefferson, A.: Measured atmospheric new particle formation rates: implication for nucleation mechanisms, Chemical Engineering Communications, 151, 53-64, https://doi.org/10.1080/00986449608936541, 1996.

Weber, R. J., Marti, J. J., McMurry, P. H., Eisele, F. L., Tanner, D. J., and Jefferson, A.: Measurements of new particle formation and ultrafine particle growth rates at a clean continental site, Journal of Geophysical Research, 102, 4375-4385, https://doi.org/10.1029/96jd03656, 1997.

Wiedensohler, A., Birmili, W., Nowak, A., Sonntag, A., Weinhold, K., Merkel, M., Wehner, B., Tuch, T., Pfeifer, S., Fiebig, M., Fjäraa, A. M., Asmi, E., Sellegri, K., Depuy, R., Venzac, H., Villani, P., Laj, P., Aalto, P., Ogren, J. A., Swietlicki, E., Williams, P., Roldin, P., Quincey, P., Hüglin, C., Fierz-Schmidhauser, R., Gysel, M., Weingartner, E., Riccobono, F., Santos, S., Grüning, C., Faloon, K., Beddows, D., Harrison, R., Monahan, C., Jennings, S. G., O'Dowd, C. D., Marinoni, A., Horn, H. G., Keck, L., Jiang, J., Scheckman, J., McMurry, P. H., Deng, Z., Zhao, C. S., Moerman, M., Henzing, B., de Leeuw, G., Löschau, G., and Bastian, S.: Mobility particle size spectrometers: harmonization of technical standards and data structure to facilitate high quality long-term observations of atmospheric particle number size distributions, Atmospheric Measurement Techniques, 5, 657-685, https://doi.org/10.5194/amt-5-657-2012, 2012.

Williamson, C. J., Kupc, A., Axisa, D., Bilsback, K. R., Bui, T., Campuzano-Jost, P., Dollner, M., Froyd, K. D., Hodshire, A. L., Jimenez, J. L., Kodros, J. K., Luo, G., Murphy, D. M., Nault, B. A., Ray, E. A., Weinzierl, B., Wilson, J. C., Yu, F., Yu, P., Pierce, J. R., and Brock, C. A.: A large source of cloud condensation nuclei from new particle formation in the tropics, Nature, 574, 399-403, https://doi.org/10.1038/s41586-019-1638-9, 2019.

Wu, Z., Hu, M., Liu, S., Wehner, B., Bauer, S., Ma ßling, A., Wiedensohler, A., Petäjä, T., Dal Maso, M., and Kulmala, M.: New particle formation in Beijing, China: Statistical analysis of a 1-year data set, Journal of Geophysical Research, 112, https://doi.org/10.1029/2006jd007406, 2007.

Wyslouzil, B. E., Seinfeld, J. H., Flagan, R. C., and Okuyama, K.: Binary nucleation in acid–water systems. II. Sulfuric acid–water and a comparison with methanesulfonic acid–water, The Journal of Chemical Physics, 94, 6842-6850, https://doi.org/10.1063/1.460262, 1991.

Yao, L., Garmash, O., Bianchi, F., Zheng, J., Yan, C., Kontkanen, J., Junninen, H., Mazon, S. B., Ehn, M., Paasonen, P., Sipilä, M., Wang, M., Wang, X., Xiao, S., Chen, H., Lu, Y., Zhang, B., Wang, D., Fu, Q., Geng, F., Li, L., Wang, H., Qiao, L., Yang, X., Chen, J., Kerminen, V.-M., Petäjä, T., Worsnop, D. R., Kulmala, M., and Wang, L.: Atmospheric new particle formation from sulfuric acid and amines in a Chinese megacity, Science, 361, 278-281, https://doi.org/10.1126/science.aao4839 2018.

Yao, X., Choi, M. Y., Lau, N. T., Lau, A. P. S., Chan, C. K., and Fang, M.: Growth and Shrinkage of New Particles in the Atmosphere in Hong Kong, Aerosol Science and Technology, 44, 639-650, https://doi.org/10.1080/02786826.2010.482576, 2010.

Ye, Q., Wang, M., Hofbauer, V., Stolzenburg, D., Chen, D., Schervish, M., Vogel, A., Mauldin, R. L., Baalbaki, R., Brilke, S., Dada, L., Dias, A., Duplissy, J., El Haddad, I., Finkenzeller, H., Fischer, L., He, X., Kim, C., Kürten, A., Lamkaddam, H., Lee, C. P., Lehtipalo, K., Leiminger, M., Manninen, H. E., Marten, R., Mentler, B., Partoll, E., Petäjä, T., Rissanen, M., Schobesberger, S., Schuchmann, S., Simon, M., Tham, Y. J., Vazquez-Pufleau, M., Wagner, A. C., Wang, Y., Wu, Y., Xiao, M., Baltensperger, U., Curtius, J., Flagan, R., Kirkby, J., Kulmala, M., Volkamer, R., Winkler, P. M., Worsnop, D., and Donahue, N. M.: Molecular Composition and Volatility of Nucleated Particles from α-Pinene Oxidation between −50 °C and +25 °C, Environmental Science & Technology, 53, 12357-12365, https://doi.org/10.1021/acs.est.9b03265, 2019.

Yli-Juuti, T., Riipinen, I., Aalto, P. P., Nieminen, T., Maenhaut, W., Janssens, I. A., Claeys, M., Salma, I., Ocskay, R., and Hoffer, A.: Characteristics of new particle formation events and cluster ions at K-puszta, Hungary, Boreal Environment Research, 14, 683-698, 2009.

Yli-Juuti, T., Nieminen, T., Hirsikko, A., Aalto, P. P., Asmi, E., Hõrrak, U., Manninen, H. E., Patokoski, J., Dal Maso, M., Petäjä, T., Rinne, J., Kulmala, M., and Riipinen, I.: Growth rates of nucleation mode particles in Hyytiälä during 2003−2009: variation with particle size, season, data analysis method and ambient conditions, Atmospheric Chemistry and Physics, 11, 12865-12886, https://doi.org/10.5194/acp-11-12865-2011, 2011.

Young, L. H., Lee, S. H., Kanawade, V. P., Hsiao, T. C., Lee, Y. L., Hwang, B. F., Liou, Y. J., Hsu, H. T., and Tsai, P. J.: New particle growth and shrinkage observed in subtropical environments, Atmospheric Chemistry and Physics, 13, 547-564, https://doi.org/10.5194/acp-13-547-2013, 2013.

Yu, F., and Luo, G.: Simulation of particle size distribution with a global aerosol model: contribution of nucleation to aerosol and CCN number concentrations, Atmospheric Chemistry and Physics, 9, 7691-7710, https://doi.org/10.5194/acp-9-7691-2009, 2009.

Zhang, J., Chen, Z., Lu, Y., Gui, H., Liu, J., Wang, J., Yu, T., and Cheng, Y.: Observations of New Particle Formation, Subsequent Growth and Shrinkage during Summertime in Beijing, Aerosol and Air Quality Research, 16, 1591-1602, https://doi.org/10.4209/aaqr.2015.07.0480, 2016.